Stellar Ages for Galactic Archaeology

Methods and Applications

Sahlholdt, Christian

2021

Document Version:
Publisher's PDF, also known as Version of record

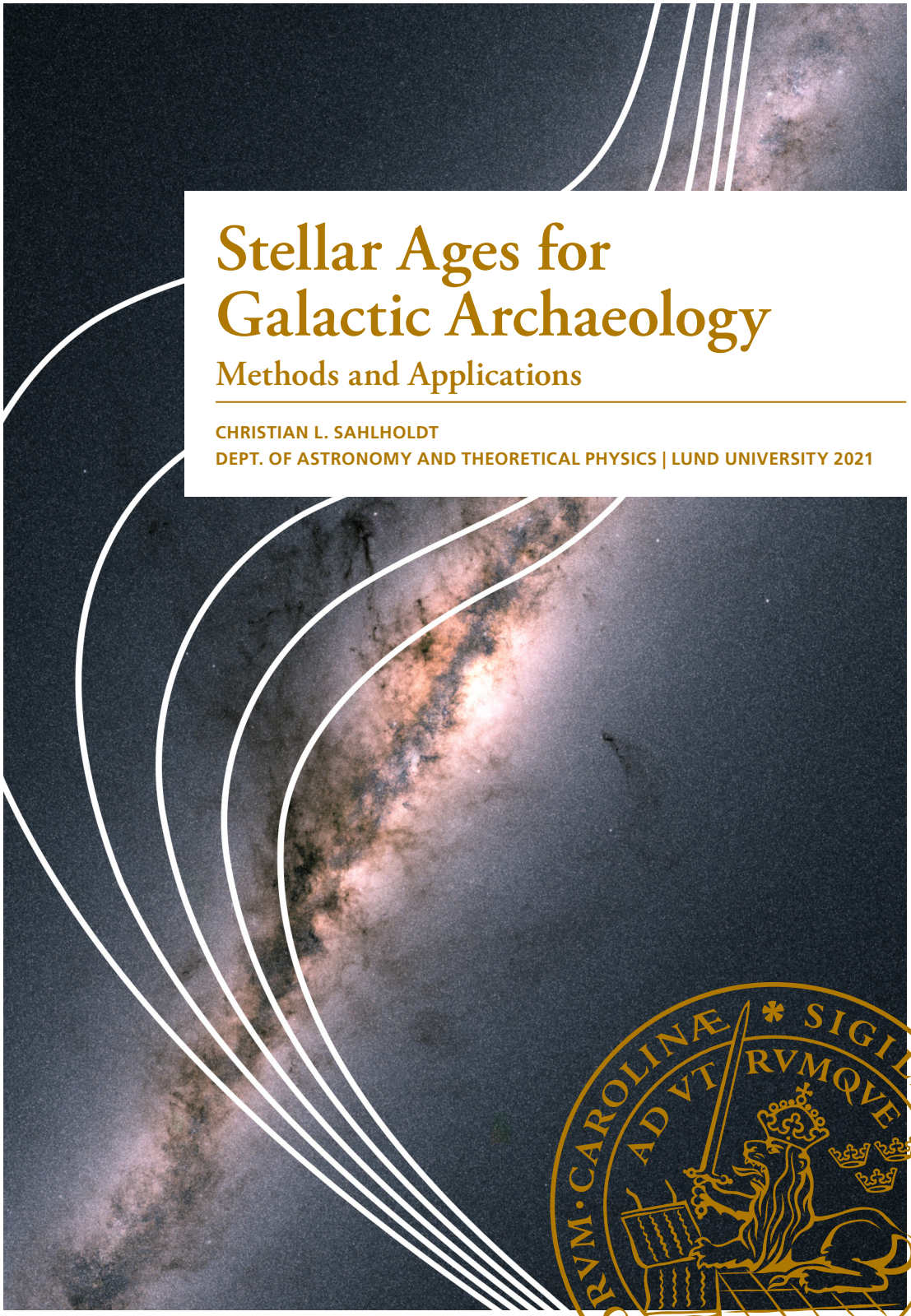

Stellar Ages for Galactic Archaeology

Methods and Applications

CHRISTIAN L. SAHLHOLDT
DEPT. OF ASTRONOMY AND THEORETICAL PHYSICS | LUND UNIVERSITY 2021

Printed by Media-Tryck, Lund 2021 NORDIC SWAN ECOLABEL 3041 0903

Faculty of Science
Department of Astronomy
and Theoretical Physics

ISBN 978-91-7895-931-0

Stellar Ages for Galactic Archaeology

Stellar Ages for Galactic Archaeology

Methods and Applications

Christian L. Sahlholdt

LUND
UNIVERSITY

Thesis for the degree of Doctor of Philosophy

Thesis advisor: Prof. Sofia Feltzing
Co-advisors: Dr. Diane Feuillet, Dr. Oscar Agertz
Faculty opponent: Prof. Heidi Jo Newberg

To be presented, with the permission of the Faculty of Science of Lund University, for public criticism in the Lundmark lecture hall (Lundmarksalen) at the Department of Astronomy and Theoretical Physics on Friday 1st October 2021 at 15:00.

Organization	Document name
LUND UNIVERSITY	**DOCTORAL DISSERTATION**
Department of Astronomy and Theoretical Physics Box 43, SE-22100 Lund, Sweden	**Date of issue** 2021-09-06
Author(s) Christian L. Sahlholdt	Sponsoring organization

Title and subtitle
Stellar Ages for Galactic Archaeology: Methods and Applications

Abstract
Galactic Archaeology is the study of the formation and evolution of the Milky Way through the properties of stars and stellar populations. The combination of stellar ages, chemical compositions, positions, and velocities can reveal the history of star formation and chemical enrichment in different regions of the Galaxy. A large number of stellar spectroscopic, photometric, and astrometric surveys are currently providing the data necessary to determine the properties of millions of stars spanning almost the entire distance from the Galactic centre to its outskirts. These data do not give stellar ages directly, but ages can be estimated by comparing the surface properties of the stars with models of stellar evolution.

This thesis covers the work presented in five papers concerning stellar ages for studies of Galactic Archaeology. In Paper I, we investigate the ages of the *Gaia* benchmark stars, a sample of 33 nearby stars used as a validation sample in large surveys. By combining new age estimates from model fitting with age estimates found in the literature, we define benchmark ages for 16 of the stars. In Paper III we present a new method for estimating the sample age-metallicity distribution (SAMD) of a population of stars. This method combines the full age-metallicity probability density functions from model fitting of individual stars and is found to yield more precise age distributions than the distribution of individual age estimates.

The remaining papers are devoted to the study of the formation history of stellar populations in the Milky Way disc and halo. In Paper II we study the properties of two stellar populations in the halo and find that they formed at the same time more than 10 Gyr ago, but at significantly different metallicities. This is consistent with the prevailing interpretation that the most metal-poor population has been accreted from a dwarf galaxy and that the other population is made up of kinematically hot Milky Way disc stars. In Paper IV we revisit the age distribution of the accreted component and find it to be consistent with a single population of stars with ages in the range 10 to 12 Gyr. We also investigate the properties of a population of stars on retrograde orbits claimed to be accreted from another distinct dwarf galaxy. This population seems to be of a mixed origin as indicated, for example, by a multimodal age distribution. Finally, in Paper V we calculate the SAMD for a sample of almost 200 000 stars in the Milky Way disc. The SAMD shows two local minima, at ages of approximately 5 and 10 Gyr, indicating that the disc stars formed in three main phases. First along a single chemical evolution track in the inner disc until around 10 Gyr ago, then across the disc with outwardly decreasing metallicity, and finally in a burst of star formation 2 to 4 Gyr ago.

Key words
Galactic Archaeology; Stellar ages; Milky Way formation; Milky Way evolution; Low mass stars

Classification system and/or index terms (if any)

Supplementary bibliographical information		**Language** English
ISSN and key title		**ISBN** 978-91-7895-931-0 (print) 978-91-7895-932-7 (pdf)
Recipient's notes	**Number of pages** 210	Price
	Security classification	

Stellar Ages for Galactic Archaeology

Methods and Applications

Christian L. Sahlholdt

LUND
UNIVERSITY

Faculty Opponent

Prof. Heidi Jo Newberg
Rensselaer Polytechnic Institute,
Troy, NY, USA

Evaluation Committee

Prof. Eric Bell
Department of Astronomy, University of Michigan,
Ann Arbor, MI, USA

Prof. Saskia Hekker
Heidelberg Institute for Theoretical Studies,
Heidelberg, Germany

Prof. Maurizio Salaris
Astrophysics Research Institute, Liverpool John Moores University,
Liverpool, UK

Front cover: The Gaia satellite's view of the Milky Way. Stellar isochrones for five different ages are overlaid. Image credit: ESA/Gaia/DPAC.

Faculty of Science, Department of Astronomy and Theoretical Physics

ISBN: 978-91-7895-931-0 (print)
ISBN: 978-91-7895-932-7 (pdf)

Printed in Sweden by Media-Tryck, Lund University, Lund 2021

Media-Tryck is a Nordic Swan Ecolabel certified provider of printed material. Read more about our environmental work at www.mediatryck.lu.se

MADE IN SWEDEN

Dedicated to the memory of my grandfather

Contents

List of publications

This thesis is based on the following peer-reviewed publications:

I **Benchmark ages for the *Gaia* benchmark stars**
C. L. Sahlholdt, S. Feltzing, L. Lindegren, R. P. Church (2019)
Monthly Notices of the Royal Astronomical Society, vol. 482, pp.895-920

II **Characteristics of the Two Sequences Seen in the High-velocity Hertzsprung–Russell Diagram in *Gaia* DR2**
C. L. Sahlholdt, L. Casagrande, S. Feltzing (2019)
The Astrophysical Journal Letters, vol. 881, L10, 7 pp.

III **Estimating the age-metallicity distribution of a stellar sample from the probability distributions of the individual stars**
C. L. Sahlholdt, L. Lindegren (2021)
Monthly Notices of the Royal Astronomical Society, vol. 502, pp.845-864

IV **Selecting accreted populations: metallicity, elemental abundances, and ages of the Gaia-Sausage-Enceladus and Sequoia populations**
D. Feuillet, **C. L. Sahlholdt**, S. Feltzing, L. Casagrande (2021)
Submitted to Monthly Notices of the Royal Astronomical Society (May 2021)

V **Characterizing epochs of star formation across the Milky Way disc through age-metallicity distributions of GALAH stars**
C. L. Sahlholdt, S. Feltzing, D. Feuillet (2021)
To be submitted to Monthly Notices of the Royal Astronomical Society

Work not included in the thesis

Selected relevant publications not included in this thesis:

I **Testing asteroseismic radii of dwarfs and subgiants with Kepler and *Gaia***
C. L. Sahlholdt, V. Silva Aguirre, L. Casagrande, J. R. Mosumgaard, M. Bojsen-Hansen (2018)
Monthly Notices of the Royal Astronomical Society, vol. 476, pp.1931-1941

II **Asteroseismic radii of dwarfs: new accuracy constraints from Gaia DR2 parallaxes**
C. L. Sahlholdt, V. Silva Aguirre (2018)
Monthly Notices of the Royal Astronomical Society: Letters, vol. 481, pp.L125-L129

III **A Benchmark Age for μ Herculis**
C. L. Sahlholdt, S. Feltzing (2019)
Research Notes of the American Astronomical Society, vol. 3, 65.

IV **The HR 1614 moving group is not a dissolving cluster**
I. Kushniruk, T. Bensby, S. Feltzing, **C. L. Sahlholdt**, D. Feuillet, L. Casagrande (2020)
Astronomy & Astrophysics, vol. 638, A154, 11 pp.

V **The SkyMapper-Gaia RVS view of the Gaia-Enceladus-Sausage - an investigation of the metallicity and mass of the Milky Way's last major merger**
D. Feuillet, S. Feltzing, **C. L. Sahlholdt**, L. Casagrande (2020)
Monthly Notices of the Royal Astronomical Society, vol. 497, pp.109-124

Popular summary

The Sun is just one out of approximately 100 billion stars in our home galaxy, the Milky Way. Most of these stars are orbiting around the Galactic centre in a thin disc-like structure, and a small fraction of stars are found in the almost spherical halo in which the disc is embedded. One of the great questions of astronomy is how these structures, and the Milky Way as a whole, formed and evolved from the early universe until today.

The branch of astronomy which deals with the formation history of the Milky Way is also called Galactic Archaeology. Just like archaeologist can study ancient artefacts to learn about past civilizations, astronomers can study the properties of stars to learn about the past conditions of the Galaxy. Among the most relevant stellar properties are their ages and the abundance of metals (elements heavier than hydrogen and helium) in their atmospheres. The heavy elements did not exist in the early universe but have since been produced by stars, for example when they explode as supernovae. Therefore, the stars we observe today contain an imprint in their atmospheres left over from previous generations of stars. This can be combined with knowledge of their ages to retrace when and under which conditions star formation has taken place.

The field of Galactic Archaeology is currently very active thanks to a number of large-scale surveys observing more Milky Way stars than ever before. From the ground, large telescopes can collect spectra for up to thousands of stars at a time. Analysis of the spectra reveal the detailed composition of metals in the stars. From space, the *Gaia* spacecraft is recording the positions and velocities of more than a billion stars. The focus of this thesis is on estimating stellar ages for use in Galactic Archaeology in combination with the vast amount of data now available from these large surveys.

The ages of individual stars can be estimated by comparing their observed properties with stellar models. Using this method, we study the ages of 33 nearby bright stars. For about half of these stars we are able to give a well-defined age which can be used as a reference for future studies. We also present a new statistical method for obtaining more precise age distributions for large samples of stars with different levels of heavy elements.

We have used the new method to study the ages of stars in both the halo and disc of the Milky Way. The halo contains some of the oldest and most metal-poor stars in the Galaxy which trace the very early formation history. Recently, it was found that a large number of halo stars were formed in a dwarf galaxy which since collided with the Milky Way. We find that these stars formed more than 10 billion

years ago at the same time as the first stars were forming in the inner parts of the Milky Way disc. By considering the disc as a whole, we find that star formation has proceeded in three main phases. First in the inner disc with a continuous increase in heavy elements, then across the disc with lower heavy element abundances in the outer disc, and finally in a recent burst of star formation.

Most of the results presented in this thesis have only become possible to obtain within the past decade thanks to the many large-scale stellar surveys. Many of these surveys are still ongoing, and many more are being planned for the future. These surveys will expand studies of Galactic Archaeology to more distant regions of the Milky Way and further improve our understanding of its formation and evolution, as well as galaxy evolution in general.

Populärvetenskaplig sammanfattning

Solen är en av de ca 100 miljarder stjärnor som finns i Vintergatan, vårt hem i universum. De flesta av dessa stjärnor rör sig i disklika banor runt Vintergatans centrum. En liten del av stjärnorna rör sig i banor som tar dem långt från Vintergatsplanet. De utgör en slags halo av stjärnor runt disken. En av de viktigaste frågorna inom astronomisk forskning är att förstå hur dessa strukturer och Vintergatan i sin helhet bildades och utvecklades från universums början till idag.

Den del av astronomin som studerar hur Vintergatan bildades kallas ofta för Galaktisk Arkeologi. Precis som arkeologen här på jorden kan studera antika artefakter och genom dessa lära sig om utdöda civilisationer kan astronomer studera egenskaperna hos stjärnorna för att lära sig om förhållandena i Vintergatan förr i tiden. Bland de viktigaste egenskaperna vi kan mäta upp för en stjärna är dess ålder och innehåll av grundämnen tyngre än helium och väte, så kallade metaller. Dessa tyngre grundämnen existerar inte i det tidiga universum utan har producerats i stjärnor, till exempel när de exploderar som supernovor. Detta innebär att de stjärnor som vi observerar idag, i sina atmosfärer, innehåller ett prov på vad tidigare stjärngenerationer har lämnat efter sig. Genom att kombinera mätningar av grundämneshalter med stjärnornas åldrar kan vi återskapa när och under vilka förhållanden som stjärnor har bildats.

Forskningsområdet är för närvarande mycket aktivt. Detta beror till stor del på de genommönstringar av Vintergatsstjärnor som genomförs nu. Från jorden kan moderna teleskop registrera spektra för tusentals stjärnor åt gången. Analys av stjärnornas spektra ger oss detaljinformation om deras grundämnessammansättning. I rymden mäter Gaia-satelliten positioner och hastigheter för mer än en miljard stjärnor. Fokus i min avhandling är att bestämma åldrar för stjärnor och att använda dem tillsammans med data från de stora jordbaserade spektroskopiska genommönstringarna.

En stjärnas ålder kan bestämmas genom att jämföra deras observerade egenskaper med modellförutsägelser. Genom att använda denna metod - dvs jämföra observationer med modeller - har vi studerat åldern hos 33 ljusstarka stjärnor. För ca hälften av dessa kan vi bestämma en väldefinierad ålder som kan användas som referenspunkter i framtida studier. Vi har också presenterat en ny statistisk metod för att ta fram mer precisa åldersfördelningar för många stjärnor på en gång. Metoden tar hänsyn till att stjärnorna kan ha olika halter av tunga grundämnen.

Vi har använt vår nya metod för att studera åldersfördelningarna hos stjärnor i Vintergatans disk och halo. Stjärnhalon innehåller några av de allra äldsta stjärnorna som dessutom har mycket lite av de tyngre grundämnena. Dessa stjärnor ger en

inblick i de allra första stadierna av Vintergatans tillblivelse. Nyligen har forskare funnit en stor mängd stjärnor som ursprungligen bildades i en dvärggalax men som senare har kolliderat med och sammansmält med Vintergatan. I vår studie finner vi att dessa stjärnor bildades för mer än 10 miljarder år sedan och att samtidigt bildades det också stjärnor i Vintergatans inre delar. Om vi betraktar Vintergatans stjärndisk i sin helhet finner vi att stjärnbildningen har skett i väsentligen tre faser. Först i den inre disken med stadigt ökande mängder av tyngre grundämnen, sedan i hela disken men nu med en något lägre mängd av tunga grundämnen och slutligen i en sen ”burst” av stjärnbildning.

Resultaten som jag lägger fram i min avhandling har bara varit möjliga att erhålla under de senaste tio åren tack vare de stora genommönstringarna av Vintergatans stjärnor. Flera genommönstringar pågår fortfarande och ytterligare är planerade för framtiden. Dessa genommönstringar kommer att möjliggöra arkeologiska studier på större och större avstånd i Vintergatans yttre regioner och hjälpa oss att förstå hur vår hemgalax bildades och utvecklades. Dessa resultat kommer vara viktiga för vår förståelse av galaxbildning i gemen.

Acknowledgements

I want to thank my main supervisor Sofia Feltzing for giving me the opportunity to continue my studies in astronomy and for providing helpful guidance along the way. I appreciate your continued support and being granted the independence to also pursue a few side projects along with the thesis. Similarly, I am grateful for the support of my co-supervisors Diane Feuillet and Oscar Agertz. Diane played an important part in shaping my final projects and I very much enjoyed our discussions and collaborations in the last couple of years of my studies. Given more time I would have liked to look more closely at galaxy simulations with the help of Oscar. Now I look forward to following the progress of the field in the future.

The computational side of this thesis would not have been possible without the initial code provided by Lennart Lindegren and Louise Howes. I am very thankful for your support which helped me get started when I first arrived in Lund. Without it I am sure this work would have taken much longer to complete.

I also want to extend my gratitude to all of the students and staff of Lund Observatory for making it a nice place to study and work. It is an interesting experience to spend a few years in an academic environment where people come and go with every season. Throughout it all, I can safely say that the observatory has hosted some of the most kind and welcoming people I have had the pleasure of meeting. One of the constants through the years has been my office mate Timmi Jørgensen with whom I have been happy to get to speak some Danish on a regular basis.

I am grateful to my friend Lasse Sandström (and Sisko) for providing me comfortable accommodation for my time in Lund. Your photobook about the town is the perfect memento for my time spent here. Now I can finally return the favour with a copy of my own work.

Finally, I want to thank my family for always being supportive of me and my work. A special thanks goes out to my dad who is always among the first to read my scientific publications, even if only the introduction.

Stellar Ages for Galactic Archaeology: Methods and Applications

1 Introduction

One of the big questions in astronomy is how galaxies form and evolve. To get a better understanding of this subject, a great deal of insight can be gained by studying our home galaxy, the Milky Way. From our vantage point inside the Galactic disc we can study individual stars and stellar populations in extensive detail. If we manage to understand how the stellar populations of the Milky Way formed, the results can likely be generalized to other similar galaxies.

The Milky Way is a disc galaxy and is classically divided into three main components: the disc, the bulge, and the halo (Bland-Hawthorn & Gerhard, 2016) (see Figure 1). Stars in the disc, including the Sun, move on more or less circular orbits around the Galactic centre. The disc can be further divided into a thin and thick component that were initially defined based on the observation of a break in the vertical density distribution of stars (Gilmore & Reid, 1983). Stars in the thick disc – the component that extends furthest from the disc plane – are older and more metal-poor than thin disc stars. The bulge is located at the centre of the Galaxy and appears as a thickening of the disc. Finally, the halo surrounds the disc and contains some of the oldest and most metal-poor stars in the Galaxy. Halo stars can be identified in the Solar neighbourhood by their large velocities relative to the circular velocity of the disc.

The formation history of the various Galactic structures can be investigated by studying their stars, a discipline also called Galactic Archaeology (Freeman & Bland-Hawthorn, 2002). In this cosmic branch of archaeology, the stars make up

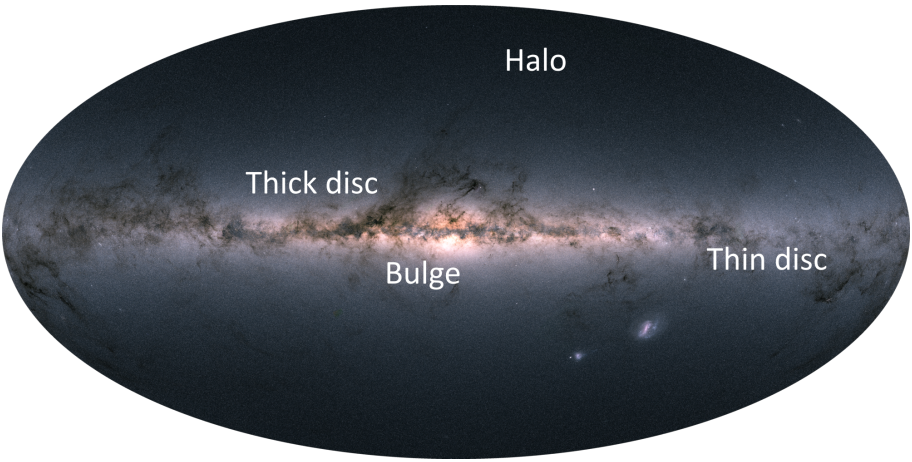

Figure 1: Map of point sources (mainly stars) in the Milky Way observed by the *Gaia* spacecraft. The main structural components are indicated schematically. Image adapted from *Gaia* Data Processing and Analysis Consortium (DPAC) (CC-BY-SA 3.0 IGO).

the fossil record. With each successive generation of star formation, the interstellar medium is enriched in heavy elements by the products of stellar nucleosynthesis. This chemical enrichment can be traced through the chemical compositions of the stars we see today. Additionally, the orbit of a star contains information about its kinematic history and can be used, for example, to distinguish between stars from different components of the Milky Way or to identify stars that have formed in an external galaxy and since accreted onto the Milky Way (Helmi, 2020). To complete the fossil record it is necessary to know the ages of the stars. Stellar ages are one of the most challenging properties to estimate precisely (Soderblom, 2010) but they put crucial constraints on the timeline of star formation and chemical enrichment.

In recent years, the availability of stellar data from large spectroscopic, photometric and astrometric surveys has increased significantly. This survey data enables studies of the elemental abundances and kinematics of millions of stars in the Solar neighbourhood and beyond. It also enables age estimation for a large number of field stars based on e.g. fitting stellar evolution models to the observed surface properties of the stars. The combination of precise spectroscopic data and distance estimates has made it possible to estimate ages for millions of field stars in the volume around the Sun (Sanders & Das, 2018).

The work presented in this thesis touches on a variety of topics united under

the subject of Galactic Archaeology and with a common focus on age estimation for stars observed in large surveys. It can be roughly divided into two main topics. The first topic is stellar age estimation, using model fitting, both for individual field stars and for large populations of stars in the Galaxy. The second topic is the investigation of the formation history of some of the main components of the Milky Way by combining this age information with the elemental abundances and kinematics available for large samples of stars. The following sections give a summary of the data and methods applied in this work as well as the main results we have obtained. The full research papers are reproduced in the second part of the thesis.

2 Survey data

The detailed study of stellar populations in the Milky Way relies on data from a wide variety of sources. The work presented in this thesis is based on data from a number of large spectroscopic, photometric, and astrometric surveys. In the following, the main sources of data, which will be referred to in later sections, are summarised.

2.1 Spectroscopy

Elemental abundances of stars can be determined by studying the absorption lines in stellar spectra. Knowledge of elemental abundances is important in its own right in studies of Galactic chemical evolution, but the metallicity, [Fe/H][1], and abundance of alpha elements, [α/Fe], are also crucial for age estimation of individual stars due to model degeneracies between age and chemical composition (see e.g. the discussion in Howes et al., 2019). Spectra also provide the effective temperatures, $T_{\rm eff}$, and radial velocities of stars.

The bulk of the spectroscopic data used in this work comes from two large ground-based high-resolution spectroscopic surveys: the Apache Point Observatory Galactic Evolution Experiment (APOGEE; Majewski et al., 2017) and the Galactic Archaeology with HERMES survey (GALAH; De Silva et al., 2015). Each of these surveys have observed and analysed about half a million stars and aim to provide abundances for up to 30 elements.

The APOGEE survey operates at near-infrared wavelengths and mainly targets giant stars which allows for observations of stars in a large volume of the Galaxy, out to distances of more than 5 kpc. Since 2017 APOGEE has been collecting spectra from two sites allowing for observations in both the northern and southern hemisphere. The latest release of APOGEE data is Data Release 16 (DR16; Ahumada et al., 2020; Jönsson et al., 2020) which also includes the first results from the Southern survey.

The GALAH survey operates at visual wavelengths in the Southern hemisphere and focuses on the Galactic disc. Most of the GALAH targets are within 2 kpc of the Sun and are divided almost equally between dwarf and giant stars. The most recent data release from GALAH is Data Release 3 (DR3; Buder et al., 2021).

[1] The bracket notation is shorthand for the relative abundance of elements on a logarithmic scale normalized to the Solar value, i.e. $[\mathrm{Fe/H}] \equiv \log_{10}\left(n(\mathrm{Fe})/n(\mathrm{H})\right) - \log_{10}\left(n(\mathrm{Fe})/n(\mathrm{H})\right)_{\odot}$.

2.2 Photometry

Photometric surveys provide the apparent magnitudes of stars in different passbands. The Two Micron All Sky Survey (2MASS; Skrutskie et al., 2006) observed the entire sky in the three near-infrared bands J, H, and K_s resulting in a catalogue of over 400 million point sources. Magnitudes from the 2MASS K_s band are applied in several places in this thesis, e.g. to estimate stellar ages in combination with spectroscopic data. This band is chosen since it is less sensitive to extinction due to interstellar dust than bands in the visual wavelength range.

Magnitudes are not the only parameters obtained from photometric surveys. Some photometric systems, such as the Strömgren uvbyβ system, are sensitive to stellar effective temperatures and metallicities (Strömgren, 1966). A Strömgren-like system is used by the SkyMapper Southern Sky Survey. Casagrande et al. (2019) used the SkyMapper photometry to estimate metallicities for about 9 million stars in the southern hemisphere. They used stars in common with the GALAH survey to calibrate the relation between photometry and metallicity.

2.3 Astrometry

Astrometry is the study of the positions of celestial objects. The number of Milky Way stars with precise astrometric observations has increased significantly in recent years thanks to the *Gaia* spacecraft (Gaia Collaboration et al., 2016) launched in 2013. *Gaia* scans the entire sky periodically from its orbit around the Sun. It records the magnitudes and positions of stars over time with the objective of creating a three-dimensional map of the Milky Way.

Following the second *Gaia* data release (DR2; Gaia Collaboration et al., 2018a) positions, proper motions, and parallaxes are available for more than a billion stars in the Milky Way. The early data release 3 (EDR3; Gaia Collaboration et al., 2021) recently updated the precision of these parameters.

The parallax, ϖ, is the apparent motion of a star caused by the shifting perspective as *Gaia* orbits around the Sun. It is related to the distance in parsec by the relation $d = 1/\varpi$, with the parallax in arcseconds. The nonlinear transformation between parallax and distance means that the distance estimate may be significantly biased if the parallax has a large uncertainty (Astraatmadja & Bailer-Jones, 2016). Therefore, studies using the *Gaia* parallaxes for distance estimates often limit the sample to the stars with relative parallax precision better than 20 per cent. Another solution is to use distance estimates calculated by combining *Gaia* parallaxes with some prior information such as the expected density profile of the

Milky Way (Bailer-Jones et al., 2018; Schönrich et al., 2019).

Gaia is also equipped with a radial velocity spectrometer and is able to measure radial velocities for the brightest stars, amounting to about 7 million in DR2. The combination of positions, proper motions, parallaxes, and radial velocities (either from *Gaia* itself or from ground-based spectroscopy) can be used to estimate the three-dimensional positions and velocities of stars. These can be used in combination with a model of the Milky Way gravitational potential to estimate orbits in the Galaxy. Such calculations have become very accessible thanks to publicly available codes such as the Python package `galpy` (Bovy, 2015).

The impact of *Gaia* on contemporary studies of stellar populations in the Milky Way cannot be overstated. As a testament to this, only Paper I in this thesis does not include any *Gaia* data. All remaining papers use some combination of the astrometry, photometry, and radial velocities from DR2 or EDR3 either for estimating stellar kinematics, ages, or both.

3 Individual stellar age estimates

Stellar age estimates are a crucial complement to the survey data in studies of Galactic Archaeology. In this thesis, the focus is on age estimates of the stars observed as part of photometric or spectroscopic surveys. Most of these are field stars, i.e. they are not associated with a cluster, and the age of each star must be assessed individually. Different age estimation methods exist for individual stars, but no single method works well for stars of all evolutionary stages (Soderblom, 2010). The most widely applicable method is model fitting, in which the age is estimated by comparing the observed stellar parameters, such as $T_{\rm eff}$, [Fe/H], and absolute magnitude, with models of stellar evolution. This method can be applied to almost all the stars observed by large surveys; however, it does not necessarily provide a precise age estimate for every star.

A stellar model describes the internal structure and surface parameters of a star with initial mass $m_{\rm ini}$ and initial total metallicity $\zeta = [{\rm M/H}]_{\rm initial}$ at a given age τ. Figure 2a shows a number of stellar models in a Hertzsprung–Russell (HR) diagram along with 500 stars selected at random from GALAH DR3. The models are plotted as isochrones – models of different masses grouped by age and initial metallicity – obtained from the PARSEC model library[2] (Bressan et al., 2012). The absolute K_s magnitudes of the GALAH stars are calculated from the apparent magnitudes, m_{K_s}, as

$$M_{K_s} = m_{K_s} - A_{K_s} - 5\log_{10}\left[(100\,{\rm mas})/\varpi\right] \ , \tag{1}$$

where the extinction, A_{K_s}, is taken from the GALAH catalogue and the parallax, ϖ, is taken from *Gaia* EDR3. Historically, stellar ages were often estimated either by eye in an HR diagram like Figure 2a or by interpolating between stellar models to the observed [Fe/H], $T_{\rm eff}$, and magnitude (e.g. Ng & Bertelli, 1998; Valenti & Fischer, 2005). Today more statistically robust methods are used, the most common being Bayesian model fitting.

3.1 Bayesian model fitting

Bayesian model fitting was introduced and popularized by Pont & Eyer (2004) and Jørgensen & Lindegren (2005a) as a way to determine statistically robust stellar ages and associated uncertainties. The version described in the following is based on the implementation by Howes et al. (2019).

[2] At the time of writing, PARSEC stellar evolution models are available through the web interface at `http://stev.oapd.inaf.it/cgi-bin/cmd`

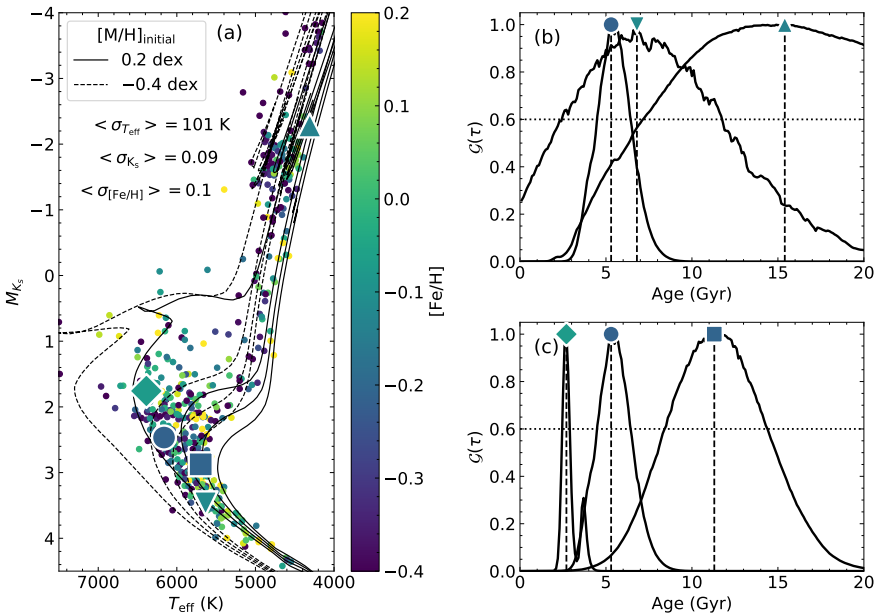

Figure 2: (a) Hertzsprung–Russell diagram of 500 GALAH DR3 stars coloured by their metallicity. PARSEC isochrones (Bressan et al., 2012) are plotted for two different initial metallicities and four ages: 2, 6, 10, and 14 Gyr. The younger isochrones have a hotter turnoff. The mean observational uncertainty on $T_{\rm eff}$, $\rm K_s$, and $\rm [Fe/H]$ are given in the panel. (b) $\mathcal{G}$ functions (marginal likelihood distributions for the age) of three stars in different stages of evolution marked by big symbols in panel a. The mode of the distributions, which can be used as the age estimate, are marked by the same symbols and by vertical dashed lines. Approximate 16 and 84 per cent confidence limits on the age estimate are given by the points of intersection with the horizontal dotted line. (c) Like panel b, but for three turnoff stars.

In addition to the initial mass, $m_{\rm ini}$, initial metallicity, ζ, and age, τ, which are intrinsic model parameters, the distance modulus, $\mu = m - M$, can be added as an external parameter defining the distance (or parallax) and apparent magnitude, $m = \mu + M$, of the model. The likelihood of observing parameters $\mathbf{x}$, with Gaussian uncertainties $\boldsymbol{\sigma}$, if the stellar model represents the true star, is given by

$$L(\mathbf{x}|\tau, \zeta, m_{\rm ini}, \mu) = \exp\left[-\frac{1}{2}\sum_i \left(\frac{x_i - X_i(\tau, \zeta, m_{\rm ini}, \mu)}{\sigma_i}\right)^2\right] , \qquad (2)$$

where $X_i(\tau, \zeta, m_{\rm ini}, \mu)$ is the model prediction of the observable x_i. A constant depending only on $\boldsymbol{\sigma}$ has been omitted from the likelihood. Since the observables are assumed to have Gaussian uncertainties it is best to avoid using the absolute magnitude as calculated from Eq. (1) because of the nonlinear transformation from parallax. Instead, the observables can be taken to be $\mathbf{x} = (T_{\rm eff}, [{\rm Fe/H}], m_{\rm K_s}, \varpi)$, including the parallax directly as a constraint on the distance modulus of the model. The likelihood can of course be calculated for any set of observables that the models can predict and it is not uncommon to use magnitudes from different passbands, a colour index instead of $T_{\rm eff}$, or the surface gravity instead of (or in addition to) the magnitude and parallax.

In stellar models, the initial metallicity is typically given by $\zeta = [{\rm M/H}]_{\rm initial} \equiv \log_{10}(Z/X) - \log_{10}(Z/X)_\odot$, i.e. the abundance fraction of all elements heavier than helium to hydrogen, scaled to the Solar value. This is equivalent to the observed [Fe/H] only as long as the star has the same relative heavy element abundances as the Sun. If, for example, the observed star is enhanced in alpha elements, with $[\alpha/{\rm Fe}] > 0$, the observed [Fe/H] is not comparable with the model [M/H]. According to Salaris et al. (1993) this alpha enhancement can be accounted for approximately by using a stellar model with a total metallicity of

$$[{\rm M/H}] = [{\rm Fe/H}] + \log_{10}(0.638 \times 10^{[\alpha/{\rm Fe}]} + 0.362) \, . \qquad (3)$$

Rather than using alpha-enhanced stellar models, the observed total metallicity can be defined using this equation. That is, the observables are taken to be $\mathbf{x} = (T_{\rm eff}, [{\rm M/H}], m_{\rm K_s}, \varpi)$, with [M/H] calculated according to Eq. (3).

Another effect that must be taken into account is atomic diffusion which causes a difference between the initial metallicity and the surface metallicity at later times. If ignored, stellar ages may be overestimated by up to 20 per cent (Dotter et al., 2017). The model surface metallicity depends not only on the initial metallicity, but also on the initial mass and age, so it can be denoted $\zeta'(\tau, \zeta, m_{\rm ini})$.

With these details taken into account, the explicit form of the likelihood given in Eq. (2) becomes

$$
\begin{aligned}
L(\mathbf{x}|\tau,\zeta,m_{\rm ini},\mu) = \exp\Bigg[& -\frac{1}{2}\left(\frac{T_{\rm eff,obs}-T_{\rm eff}(\tau,\zeta,m_{\rm ini})}{\sigma_{T_{\rm eff,obs}}}\right)^2 \\
& -\frac{1}{2}\left(\frac{[{\rm M/H}]-\zeta'(\tau,\zeta,m_{\rm ini})}{\sigma_{[{\rm M/H}]}}\right)^2 \\
& -\frac{1}{2}\left(\frac{m_{K_s}-M_{K_s}(\tau,\zeta,m_{\rm ini})-\mu}{\sigma_{m_{K_s}}}\right)^2 \\
& -\frac{1}{2}\left(\frac{\varpi-(100\,{\rm mas})\times 10^{-0.2\mu}}{\sigma_{\varpi}}\right)^2\Bigg] .
\end{aligned}
\tag{4}
$$

Bayesian model fitting is based on Bayes' theorem which states that the posterior probability density of the model parameters is given by the likelihood multiplied by the prior probability of the model parameters. Therefore, to get a probability density function over the age, the likelihood is multiplied by prior probabilities and then marginalized over all other parameters than the age. This finally gives what Jørgensen & Lindegren (2005a) called the $\mathcal{G}$ function, i.e. the relative probability of different stellar ages

$$
\mathcal{G}(\mathbf{x}|\tau) = \int_{\zeta}\int_{m_{\rm ini}}\int_{\mu} \chi(\zeta)\xi(m_{\rm ini})\psi(\mu)L(\mathbf{x}|\tau,\zeta,m_{\rm ini},\mu){\rm d}\zeta{\rm d}m_{\rm ini}{\rm d}\mu\,. \tag{5}
$$

In all applications in this work, the initial mass prior is the Salpeter initial mass function, $\xi(m_{\rm ini}) = m_{\rm ini}^{-2.35}$ (Salpeter, 1955). Other initial mass functions could be applied, but they are not significantly different from the Salpeter function in the limited range of masses considered in this work. The priors on initial metallicity and distance modulus, $\chi(\zeta)$ and $\psi(\mu)$, are kept constant.

Figure 2b shows three examples of $\mathcal{G}$ functions for stars highlighted in the HR diagram in Figure 2a. These three stars represent different stages of evolution: One example star is on the main sequence, another is on the turnoff, and the final one is on the giant branch. The most precise age estimate is obtained for the turnoff star. For this star the age, estimated as the mode of the $\mathcal{G}$ function, is $\tau = 5.30$ Gyr. Assuming the $\mathcal{G}$ function is a Gaussian, the uncertainty can be estimated as half the width of the $\mathcal{G}$ function at a value of about 60 per cent of the mode, in this case $\sigma_\tau = 0.95$ Gyr. This gives a relative age uncertainty of $\sigma_\tau/\tau \approx 18$ per cent. Relative age uncertainties at the level of 20 per cent is

about what can be expected for turnoff stars with the precision of stellar parameters from the combination of spectroscopic surveys and *Gaia*. Further down the main sequence, or on the giant branch, the isochrones are not as well separated as on the turnoff. This causes wider $\mathcal{G}$ functions, as seen in Figure 2b, and less precise age estimates. For the main sequence example, the relative age uncertainty is about 68 per cent and for the giant it seems that only a lower limit can be put on the age. This effectively limits the application of Bayesian model fitting for age estimation to turnoff and subgiant stars.

Even on the turnoff there is significant variation in the precision of age estimates. Figure 2c shows three $\mathcal{G}$ functions for turnoff stars of different ages. From young to old, the age estimates become less precise in both absolute and relative terms.

3.2 Asteroseismology

More precise age estimates can be obtained for stars showing solar-like oscillations, including giant stars. Solar-like oscillations are observed as a range of nearly equally spaced peaks in the power spectrum of the stellar light curve. These peaks represent stochastically excited pulsation modes. The mean frequency separation between the modes is related to the density of the star and the frequency of maximum power is related to its surface gravity (Chaplin & Miglio, 2013). These two parameters constrain the mass of the star which in turn constrains the age. Ages estimated in this way are often referred to as seismic ages. Seismic ages of giant stars have relative precisions down to about 20 per cent (Silva Aguirre et al., 2018), matching the precision of turnoff stars without seismology.

The challenge with solar-like oscillations is that their amplitudes are so small that it requires long continuous photometric observations to detect and characterize them. So far only the Kepler spacecraft has provided the data necessary to detect solar-like oscillations in thousands of stars (Pinsonneault et al., 2014). Even though the number of stars with seismic data is still relatively low, the Kepler seismic ages have been used extensively to calibrate other age estimation methods for giant stars. For example, machine learning methods, trained on seismic ages, have been developed to estimate ages for more than 100 000 giant stars based on the carbon and nitrogen features in their spectra (Ness et al., 2016; Ho et al., 2017). These age estimates are less precise, however, with typical relative uncertainties of around 40 per cent.

3.3 Rotation and activity-based ages

Ages of low-mass main sequence stars can be estimated based on their rotation rate using the method called gyrochronology (Barnes, 2003). All low-mass stars have convective outer layers, and this convective motion interacts with the stellar rotation to sustain a magnetic field. The resulting magnetic activity leads to stellar winds that carry off angular momentum and causes the rate of rotation to decrease. Thus, older stars are expected to show lower rates of rotation. As the star spins down, the magnetic field strength also decreases. This leads to a secondary relation between chromospheric activity and age (chromochronology).

The utility of gyro- and chromochronology is limited partly by our ability to calibrate the relations between rotation rate, or activity level, and age. The most extensive calibrations of the methods have used stars in open clusters (e.g. Mamajek & Hillenbrand, 2008). All stars in a cluster can be assumed to be born at the same time, so a single isochrone can be fitted to the cluster HR diagram in order to constrain the ages of the low-mass main-sequence stars. However, most open clusters are young which limits the calibration of the relation to stars with ages of a few gigayears. A few studies of rotation rates in older clusters have indicated that gyrochronology is applicable up to the Solar age, i.e. about 4.5 Gyr (Meibom et al., 2015; Barnes et al., 2016). On the other hand, older field stars with seismic age estimates have been found to deviate from the open cluster activity-age relation (Angus et al., 2015). This discrepancy has been attributed to a possible weakened magnetic braking for stars past the halfway-point of their main-sequence lifetime (van Saders et al., 2016).

To summarise, gyro- and chromochronology provide a means of estimating ages of low-mass main-sequence stars, but the methods may be limited to stars of roughly Solar age or younger.

3.4 Benchmark stellar ages

When studying small samples of stars it is possible to assess the quality of each individual age estimate. For model fitting this can be done by visually inspecting the $\mathcal{G}$ functions like in Figure 2b,c. However, this is not possible when working with samples of hundreds of thousands of stars. If the automatic age estimation produces spurious results for parts of the sample it may be overlooked. The same challenge exists for stellar parameters from large spectroscopic surveys. Stellar parameters determined by automatic pipelines, often involving machine learning, must be verified or calibrated against a well-characterized reference sample.

One such reference sample is called the *Gaia* benchmark stars (Jofré et al., 2014; Heiter et al., 2015). This is a sample of 33 nearby, bright stars selected to be representative of the main Galactic stellar populations, i.e. it includes dwarfs, subgiants, and giants with a range of metallicities and temperatures. Since the stars in this sample are meant as a starting point for calibrating spectroscopic data, their effective temperatures and surface gravities have been estimated independently from spectroscopy using their angular diameters and bolometric fluxes. In Paper I we assessed the ages of the *Gaia* benchmark stars. The paper had two main aims: Firstly, to test the limits of Bayesian model fitting on a set of nearby stars with high-quality parameters, and secondly to investigate the possibility of determining benchmark ages for this sample of stars.

A compilation of ages for the benchmark star μ Ara is shown in Figure 3.[3] The age estimates labelled "This work" are based on Bayesian model fitting using three different sets of stellar models: PARSEC (Bressan et al., 2012), YY (Demarque et al., 2004), and MIST (Choi et al., 2016; Dotter, 2016). For each set of stellar models the age has been estimated following the method described in Section 3.1 with data $\mathbf{x} = (T_{\rm eff}, [{\rm M/H}], m_V, \varpi)$ (subscript "magV") or $\mathbf{x} = (T_{\rm eff}, [{\rm M/H}], \log g)$ (subscript "logg"). For this star, and for most of the other dwarfs and subgiants in the sample, these six age estimates agree to within roughly 1 Gyr. For μ Ara the scatter is within the statistical uncertainties on the individual age estimates, but this is not the case for every star in the sample. For the turnoff star β Hyi, the scatter – also around 1 Gyr – is larger than the individual uncertainties. The literature age estimates for μ Ara based on model fitting show a larger scatter, from 4 to 10 Gyr (with the extreme values reported by Ibukiyama & Arimoto, 2002; Schönrich & Bergemann, 2014), likely reflecting the diversity of stellar models, fitting methods, and observational parameters used. This scatter is also greater than the statistical uncertainties which in most cases are below 1 Gyr.

These results highlight the difficulty of determining accurate stellar ages, partly due to uncertainties in stellar modelling. Another good example of the accuracy limit is the spread of ages for the Solar-like star 18 Sco. 18 Sco is a solar twin – a star with physical parameters very close to those of the Sun – which enables very precise measurements of $T_{\rm eff}$ and [Fe/H] by applying high-resolution differential spectroscopy relative to the Sun. Several studies have determined $T_{\rm eff}$ and [Fe/H] of 18 Sco with values agreeing to within 20 K and 0.01 dex, respectively (Porto de Mello et al., 2014; Nissen, 2015; Tucci Maia et al., 2016; Nissen, 2016; Spina et al., 2016); yet, they report ages ranging from 3 to 5 Gyr.

[3] The complete collection of 33 age figures can be found after Paper I at the end of the thesis.

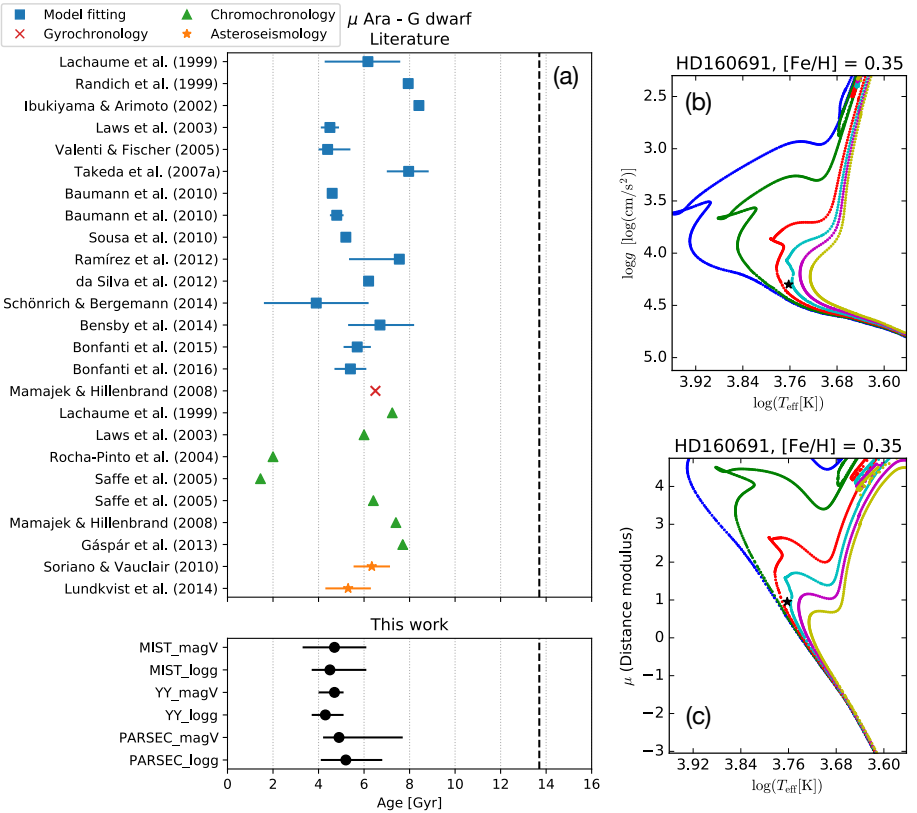

Figure 3: Ages and HR diagrams for the star μ Ara (HD 160691). (a) Ages collected from the literature (top panel), and ages determined in this work (bottom panel). The different methods used in the literature are indicated with different colours and symbols. Uncertainties on the ages are plotted for all of the literature values for which they were available, and for all ages determined in this work; however, they may be smaller than the symbol size in both cases. The vertical dashed line is to indicate the age of the Universe of 13.7 Gyr as determined by WMAP (Bennett et al., 2013). (b) Location of the star in ($T_{\rm eff}$, $\log g$)-space (star symbol) with MIST isochrones of the given metallicity and ages of 0.5, 1, 3, 6, 10, and 15 Gyr. (c) The same as panel b, but in ($T_{\rm eff}$, distance modulus)-space where the observed distance modulus is based on the parallax, and the distance modulus of the models is based on the observed apparent V magnitude. Adapted from the supporting material for Paper I.

We decided to define benchmark ages in the form of lower and upper limits to take into account both the statistical and systematic uncertainties. These age ranges are well defined for 16 out of the 33 benchmark stars and can be used for validation purposes in surveys that include observations of this sample. A major shortcoming of the sample is the fact that most of the 16 stars with well-defined ages are dwarfs and subgiants because the age constraints come mainly from model fitting. We find that for dwarf stars with $\log g > 4.4$ dex model fitting gives little to no age information. Only a single such low-mass dwarf star has been dated in the benchmark sample; namely, ϵ Eri for which several studies exist based on gyro- and chromochronology consistent with an age in the range $4 - 900$ Myr (e.g. Wright et al., 2004; Barnes, 2007; Mamajek & Hillenbrand, 2008). For the benchmark giants, strong age constraints have only been obtained for those younger than 2 Gyr. These young giants can be dated precisely because the young isochrones separate from the older ones ($\gtrsim 2$ Gyr) in the HR diagram (see Figure 3c). A future expansion of the benchmark sample to include giants with asteroseismic age constraints would be optimal to extend the sample to older giants.

Even if the absolute ages of individual stars are limited in accuracy to around 1 Gyr, the relative ages within a sample are likely more accurate. Some studies have found that ages of dwarf and subgiant stars determined with different stellar models show systematic differences of up to 1 Gyr; however, the difference is approximately constant with age for stars older than about 2 Gyr (e.g. Hayden et al., 2017; Silva Aguirre et al., 2017). This gives some confidence that relative ages of stars in similar stages of evolution are accurate to better than 1 Gyr as long as they have been homogeneously derived.

4 Stellar age distributions

When studying ages of stellar populations for Galactic Archaeology we are often more interested in the age distribution of the sample as a whole (as a proxy for the star formation history) than the ages of each individual star. In this case, it may be beneficial to combine the age information in the sample without assigning each star an individual age.

4.1 CMD fitting

One of the methods used to estimate age distributions for large samples of stars is called colour-magnitude diagram (CMD) fitting (Tosi et al., 1991; Gallart et al., 2005). This method is based on reproducing the observed CMD with a synthetic population drawn from stellar models. The star formation history is estimated by varying the contribution of different isochrones to the synthetic sample until the best match is found to the observed density of stars across the CMD.

The fact that CMD fitting requires the absolute magnitudes of entire stellar populations has limited its use mostly to dwarf galaxies (e.g. Dolphin, 2002) where all stars are at approximately the same distance. However, following the release of parallaxes from the *Hipparcos* mission (the predecessor to *Gaia*) the method has also been applied to field stars in the Milky Way (Hernandez et al., 2000). Most recently the *Gaia* data has allowed CMD fitting of about 500 000 stars in the Milky Way thick disc and halo to constrain the time of the last major merger (Gallart et al., 2019) – a topic we will return to in Section 5.

4.2 HR diagram inversion

A variant of CMD fitting was introduced as HR diagram inversion by Hernandez et al. (1999). Instead of comparing densities of stars across the CMD, this method is based on calculating the probability of any given data point being consistent with a certain model CMD described by a star formation rate SFR(τ). This probability, for a single star with $\mathcal{G}$ function $\mathcal{G}_i(\tau)$, is given by the integral in the following expression adapted from Tolstoy & Saha (1996)

$$\mathcal{L} = \prod_{i=1}^{n} \left[\int_{\tau_0}^{\tau_1} \mathrm{SFR}(\tau) G_i(\tau) \mathrm{d}\tau \right] \ . \tag{6}$$

By taking the product over all stars, Eq. (6) gives the probability of the entire sample of stars being drawn from a population with star formation rate SFR(τ). In other words, SFR(τ) can be estimated by maximising Eq. (6).

The $\mathcal{G}$ functions in the original formulation by Hernandez et al. (1999) were not based on Bayesian model fitting; instead, they used the likelihood as given by Eq. (2). They only allowed the colour to vary while keeping the luminosity and metallicity fixed. By testing the method on synthetic stellar samples they showed that various shapes of the input SFR(τ) could be recovered with good accuracy.

Following the popularization of Bayesian model fitting for age estimation, Jørgensen (2005) introduced the use of $\mathcal{G}$ functions as defined in Eq. (5) to this method. They tested the method on synthetic samples with $\mathcal{G}$ functions constrained by temperature, metallicity, and absolute magnitude, each assigned an uncertainty on the level expected from spectroscopic or photometric surveys. The recovered SFR(τ) was found to be a more accurate representation of the input than the distribution of individual ages, i.e. the histogram of age estimates derived from each individual $\mathcal{G}$ function. As discussed by Jørgensen & Lindegren (2005b), the issue with using distributions of individual ages is that the most uncertain estimates will smear out the distribution. The SFR(τ) obtained from Eq. (6) is seemingly less affected by this issue, likely because wider $\mathcal{G}$ functions contribute less probability at any specific age and are therefore less important in shaping the most likely SFR(τ). By using the full $\mathcal{G}$ functions we are also accounting for the fact that they can be bimodal or otherwise non-Gaussian; this is not accounted for when the age estimate is reduced to a single value.

Now that we have large samples of stars for which ages can be estimated, a method like the one presented above is perhaps more relevant than ever. This was the main motivation behind developing an updated and extended version of it. In Paper III we present an algorithm for estimating the sample age-metallicity distribution (SAMD) $\phi(\tau, \zeta)$ by minimising the expression

$$\begin{aligned} -\ln L' = &-\sum_i \ln\left(\int \mathcal{G}_i(\tau,\zeta)\phi(\tau,\zeta)\mathrm{d}\tau\mathrm{d}\zeta\right) \\ &+\alpha\int\left(s_\tau^2\frac{\partial^2\phi}{\partial\tau^2}+s_\zeta^2\frac{\partial^2\phi}{\partial\zeta^2}\right)^2\mathrm{d}\tau\mathrm{d}\zeta\,, \end{aligned} \tag{7}$$

where $\mathcal{G}_i(\tau, \zeta)$ is the two-dimensional $\mathcal{G}$ function of an individual star calculated using Eq. (5) but without marginalising over the metallicity. The second term is a regularisation term necessary to ensure a smooth solution. This term is regulated in strength by the parameter α, and the parameters s_τ and s_ζ act to nondimensionalise the term and set the relative strength of regularisation along the age and metallicity dimensions.

In practice, Eq. (7) is defined on a discrete grid of ages and metallicities. The expression is then minimised by calculating the derivatives with respect to the values of ϕ at each grid point and iteratively changing the values in the direction of the gradient.

By including the metallicity as a second dimension in the method, we are not attempting to derive the metallicity distribution of the sample. The metallicity is still assumed to be known for each individual star and included in the model fitting to constrain $\mathcal{G}_i(\tau, \zeta)$. The main motivation for including it is that the two-dimensional $\mathcal{G}$ function captures the correlation between age and metallicity. It is also a proof of concept to show that this method can be extended to multidimensional distributions, and there is no reason, in principle, that it cannot be further extended to add e.g. the alpha-element abundance as a third dimension. However, at present, the minimisation algorithm is not well enough optimised to add a third dimension without a significant increase in computation time or a decrease in resolution (i.e. number of grid points).

We tested the recovery of the age-metallicity distribution of various synthetic samples restricted to turnoff stars; some of these tests are shown in Figure 4. In general, for samples of at least 1000 stars, there is good qualitative agreement between the true age-metallicity distribution and the SAMD. This agreement is also seen between the true age distribution and the sample age distribution (SAD), $\phi(\tau)$, obtained by integrating the SAMD over the metallicity dimension. Even if the agreement is not perfect, the SAD is almost always an improvement over the use of histograms of individually estimated ages. This is true especially at the old end of the age distribution where the distribution of individual ages tends to flatten due to the smearing effect of the most uncertain ages.

For the tests shown in Figure 4 the regularisation parameter, α, has been tuned to achieve the best possible recovery of the input age-metallicity distribution. If α is too low, the SAMD usually shows a number of more localised spikes. For very high values of α, the SAMD goes towards a flat distribution. In Paper III we found that the optimal value of α is close to the one for which the SAMD integrated over the age dimension, $\phi(\zeta)$, is a good match to the input metallicity distribution. However, when applying it to real data from GALAH in Paper V we find very little difference in $\phi(\zeta)$ for different values of α. Therefore, we apply an alternative method based on limiting the noise in the SAMD as estimated by bootstrapping. In that way we ensure that α is large enough that the solution is not dominated by statistical fluctuations. The choice of α still leaves some ambiguity in the results, and it is important that the method is applied for a range of α-values

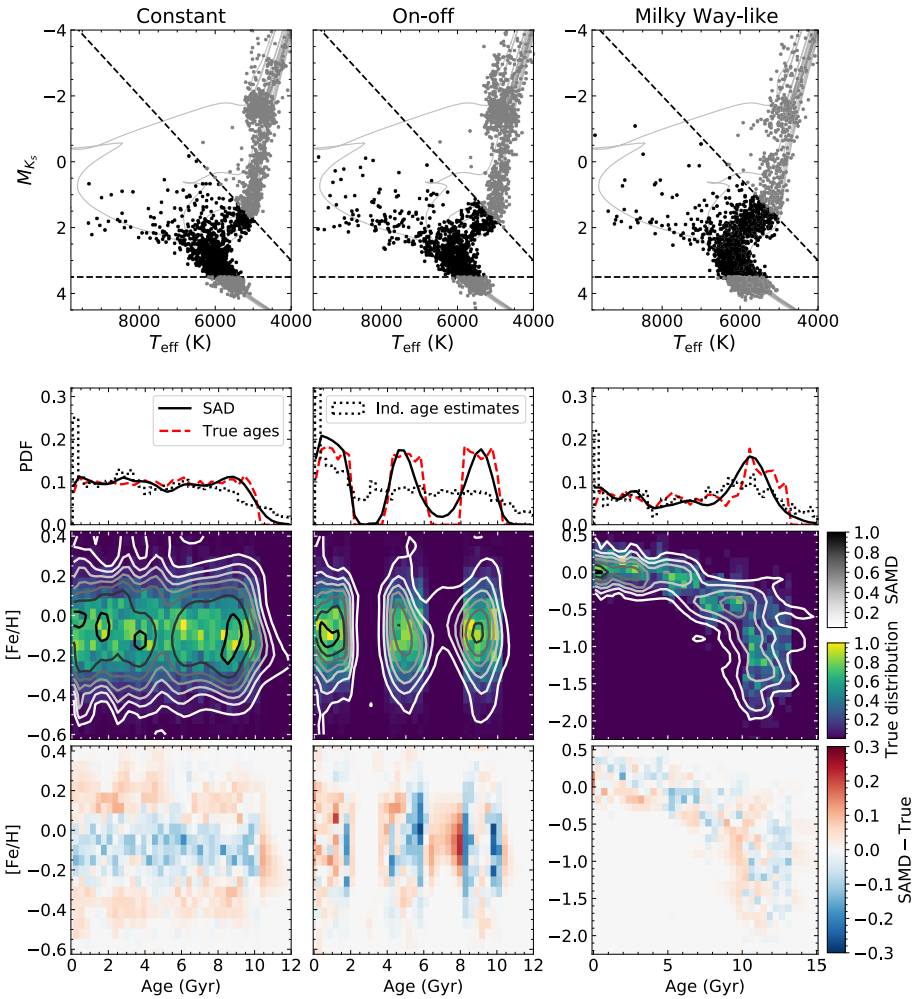

Figure 4: Tests of recovering the sample age-metallicity distribution (SAMD), using Eq. (7), for three synthetic samples with different input age-metallicity distributions. The "Constant" and "On-off" samples contain 10 000 turnoff stars and have a Gaussian distribution of metallicities centred on $[\mathrm{Fe/H}] = -0.1$ dex at all ages. The former has a flat age distribution up to 10 Gyr and the latter has a flat age distribution in the intervals 0 to 2, 4 to 6, and 8 to 10 Gyr. The "Milky Way-like" sample contains 1600 stars divided into a few subpopulations with Gaussian metallicity distributions centred on different values depending on the age following the populations of the Besançon Galaxy model (Robin et al., 2003). Only the turnoff stars highlighted in the HR diagrams are included in the test. Comparing the sample age distribution (SAD) and the distribution of individual age estimates, it is clear that the former gives a better recovery of the true age distribution. Adapted from Paper III.

in order to assess how robust features in the resulting distribution are.

Similar methods to the one discussed above have previously been presented for recovering both age distributions (Mints et al., 2019) and age-metallicity distributions (Small et al., 2013). It is difficult to compare with these methods since they are tested in different ways. In the future it would be interesting to compare our method with other similar implementations, and with CMD fitting, when applied to the same sample of stars.

5 Formation of the stellar halo

Papers I and III focused on methods for estimating individual stellar ages and age distributions. The remaining three papers focus on applying this age information in combination with elemental abundances and kinematics to study the formation of stellar populations in the Milky Way. One of these populations is the stellar halo. As mentioned in the introduction, the halo contains mainly old stars on high-velocity orbits relative to the circular velocities of disc stars. The stellar halo makes up just one per cent of the total stellar mass of the Milky Way (Bland-Hawthorn & Gerhard, 2016), but it is an important tracer of the early Milky Way formation (Helmi, 2008).

Among the first models of halo formation, the ELS model (Eggen et al., 1962) was one of the most influential. In this model the halo stars form during the rapid collapse of a large proto-galactic nebula before the gas settles into a disc. An alternative model, put forward by Searle & Zinn (1978), is that halo stars originate in protogalactic fragments that fell into the Milky Way on a longer time scale. These two classical formation scenarios for the halo are not necessarily mutually exclusive. One can imagine that the halo contains both a component formed *in situ* during the initial collapse of the Galaxy and an accreted component of stars formed outside the Milky Way progenitor. There is no doubt today that the halo contains a significant number of substructures related to accreted dwarf galaxies. One of the most well-known examples is the accreting Sagittarius dwarf galaxy (Ibata et al., 1994) which is seen as a stream of tidally stripped stars wrapping around the Milky Way (Majewski et al., 2003).

In the past few years, mainly thanks to the *Gaia* data, the number of halo field stars with precise kinematic parameters has increased significantly. Combined with the elemental abundance data from large spectroscopic surveys, this has led to new insights into the early assembly of the Milky Way halo. In this section some of these recent findings are summarised.

5.1 Two populations in the halo

Nissen & Schuster (2010) found that high-velocity stars in the Solar neighbourhood (i.e. nearby stars thought to belong to the halo) can be divided into two populations based on their detailed elemental abundances. Specifically, they found two sequences in $[\alpha/\mathrm{Fe}]$ against $[\mathrm{Fe/H}]$, at metallicities below -0.4 dex, dividing their sample into a high-alpha and low-alpha population. The relationship between $[\alpha/\mathrm{Fe}]$ and $[\mathrm{Fe/H}]$ is interesting because it reveals details about the

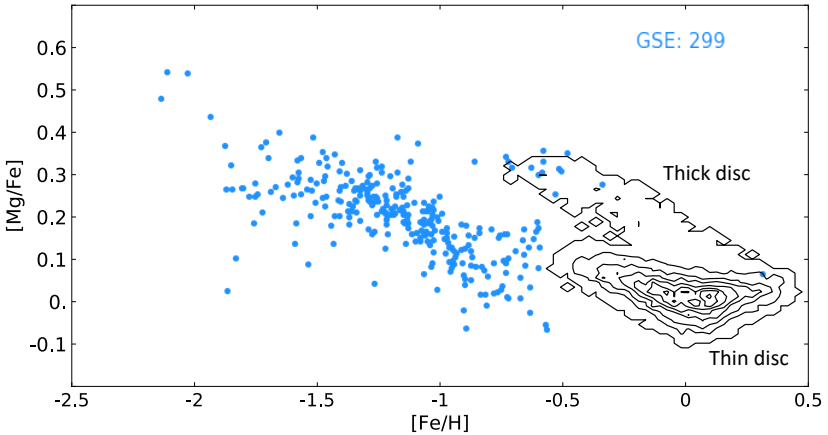

Figure 5: Magnesium to iron abundance, [Mg/Fe], against metallicity, [Fe/H], for a selection of stars in APOGEE DR16. The blue points show stars believed to have been accreted during a major merger of the Milky Way with an external galaxy dubbed the *Gaia*-Sausage-Enceladus (GSE). The black contours indicate the distribution of Milky Way stars which can be divided into an alpha-rich and alpha-poor component (in this case magnesium is the alpha element), often associated with the thick and thin discs, respectively (see Section 6 for more details about the disc components). GSE stars show a decrease in magnesium abundance at a lower metallicity than the Milky Way stars which supports the interpretation that they originate in a less massive system (see Section 5.1). Adapted from Paper IV.

early chemical evolution. At early times in the universe, the chemical enrichment is dominated by type II supernovae, resulting from the core-collapse of massive short-lived stars, that produce large amounts of alpha elements in addition to iron. Later on type Ia supernovae, resulting from exploding white dwarfs, produce significant amounts of iron causing $[\alpha/\mathrm{Fe}]$ to decrease while [Fe/H] continues to increase. The metallicity at which type Ia supernovae become dominant, and $[\alpha/\mathrm{Fe}]$ decreases, depends on the initial star formation rate and therefore the mass of the system (Tinsley, 1979). This means that halo stars accreted from dwarf galaxies less massive than the Milky Way progenitor are expected to have lower $[\alpha/\mathrm{Fe}]$ at low metallicities than stars formed *in situ* (see Figure 5). These considerations led Nissen & Schuster (2010) to conclude that their high-alpha population was formed *in situ* and that their low-alpha population had been accreted from one or more dwarf galaxies.

The presence of two halo populations became very clear following the release of *Gaia* DR2. The colour-magnitude diagram of *Gaia* stars with high velocity, defined as stars with velocity tangential to the line of sight greater than 200 km s^{-1},

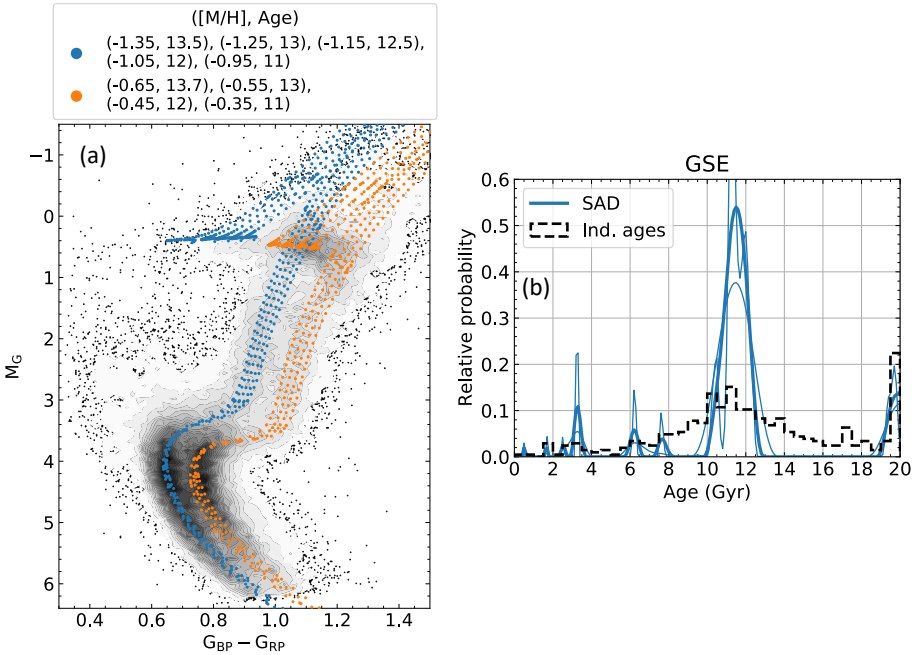

Figure 6: (a) *Gaia* DR2 CMD of 70 000 SkyMapper stars with tangential velocity (perpendicular to the line of sight) greater than 200 km s^{-1}. Isochrones fitted by eye are overlaid each of the sequences. The metallicities of the isochrones have been selected based on the SkyMapper metallicities after which the age has been adjusted to match the peak density of the turnoff. Both sequences match isochrones with ages in the range 11 to 13 Gyr, indicating that the stars formed at similar times in the early universe. (b) Distribution of individual ages and SAD for GSE stars in *Gaia* DR2 selected kinematically like the APOGEE sample shown in Figure 5. The SAD is shown for three different values of the regularisation parameter: $\alpha = 0$, 2000 (thick line), 10^5. Regardless of the level of regularisation, the SAD is consistent with the vast majority of GSE stars being formed more than 10 Gyr ago. Adapted from Paper II (panel a) and Paper IV (panel b).

split into a blue and red sequence (Gaia Collaboration et al., 2018b) (see Figure 6a). These sequences were tentatively associated with the populations found by Nissen & Schuster (2010) in the sense that the blue sequence would be made up of accreted stars and the red sequence of *in situ* stars. The interpretation of the blue sequence as a population of accreted stars was strengthened by several studies indicating that the stars follow a chemical sequence distinct from Milky Way stars (Haywood et al., 2018; Helmi et al., 2018; Mackereth et al., 2019) as also shown in Figure 5 adapted from Paper IV. Helmi et al. (2018) argue that most of the blue

sequence is made up of stars from a single object they dub the *Gaia*-Enceladus.

The blue sequence stars also stand out in terms of their kinematic properties. They have been associated with a population of stars on very radial orbits i.e. with high Galactocentric radial velocity and a distribution of azimuthal velocities centred around zero (Koppelman et al., 2018; Belokurov et al., 2018). Due to the large range of radial velocities and small absolute azimuthal velocities, the population takes on a sausage-like shape in a plot of azimuthal against radial velocity. This shape led to the name *Gaia*-Sausage for the progenitor of the accreted population. The *Gaia*-Enceladus and *Gaia*-Sausage are generally considered to be the same accreted object that is now often referred to as the *Gaia*-Sausage-Enceladus (GSE).

In Paper II we studied the two CMD sequences using a sample of 70 000 high-velocity SkyMapper stars with photometric metallicities. We defined high velocity in the same way as in the *Gaia* DR2 study, i.e. as stars with tangential velocities greater than 200 km s^{-1}. The initial aim was to estimate ages of the turnoff stars; however, the metallicity calibration was found to be unreliable for the most metal-poor dwarf and subgiant stars. Instead, we focused on stars on the red giant branch and found that the metallicity distributions of blue and red sequence stars peak at -1.4 and -0.7 dex, respectively. Isochrones were then fitted by eye to match the turnoff of the CMD sequences using metallicities around the peak values (see Figure 6a). This exercise indicated that the two sequences formed at roughly the same time, with stellar ages in the range 11 to 13 Gyr. This age range is broadly consistent with other estimates based on isochrone fitting (older than 10 Gyr; Helmi et al., 2018), the estimated time of the merger (9 to 11 Gyr ago; Di Matteo et al., 2019), and CMD fitting (half the stars were formed already 12 Gyr ago; Gallart et al., 2019). The fact that these populations formed at similar times with such different metallicities is further evidence for an accreted origin of the blue sequence stars.

In Paper IV we revisited the age distribution of the blue sequence stars, or GSE, using turnoff stars in the *Gaia* DR2 data. The *Gaia* data does not include metallicities, so we selected GSE stars from both the *Gaia* catalogue and APOGEE DR16 using the same kinematic definition as Feuillet et al. (2020). The metallicity distribution of APOGEE GSE stars was then used as a prior in the age analysis of *Gaia* turnoff stars. The resulting age distribution, shown in Figure 6b, is consistent with the previous age estimates and the SAD shows a single peak between 10 and 13 Gyr indicative of a single main population. Overall, there is now much compelling evidence that the inner parts of the Milky Way halo is dominated by

the ancient stellar debris from a single merger event.

5.2 Connection to the thick disc

As discussed in Section 5.1, the initial interpretation of the red sequence in the *Gaia* CMD was that it represents the *in situ* halo counterpart to the accreted blue sequence. However, these *in situ* halo stars are not thought to have formed during the initial collapse of the Galaxy as described by the ELS model. Instead, their kinematic properties are more consistent with a high-velocity extension of the thick disc (Bonaca et al., 2017; Haywood et al., 2018; Di Matteo et al., 2019). That is, their orbits are preferentially in the direction of disc rotation. This has led to the interpretation that the red sequence seen in the *Gaia* CMD is the heated thick disc, i.e. disc stars formed prior to the GSE merger and moved onto high-velocity orbits during it. In this interpretation there is little room for a population of halo stars formed *in situ* prior to the formation of the galactic disc. The merger heating scenario has also given this population of stars the name "the Splash" by Belokurov et al. (2020) who finds it to connect smoothly with the thick disc stars on more circular orbits in alpha-element abundances and ages. Although this is the most common interpretation in the recent literature, simulations of isolated disc galaxies have shown that a Splash-like population can form purely due to secular processes. Specifically, stars scattering off of dense clumps in the early Galaxy can lead to a kinematically hot population of old disc stars similar to the Splash (Amarante et al., 2020).

In Paper II we investigated the connection between the red sequence stars and the thick disc. First of all, we find that the maximum tangential velocity of stars in the SkyMapper sample increases monotonically as the metallicity decreases. This trend goes from the stars with low tangential velocities at high metallicities, which are clearly disc stars, down to the metallicity of -0.7 dex where a fraction of the stars, i.e. those in the red sequence, reach tangential velocities above the somewhat arbitrary halo value of 200 km s^{-1}. In this way, the red sequence looks like the tail of the velocity trend found in disc stars at higher metallicities.

Another connection between the red sequence and the thick disc is found in the spatial distribution of the stars. We assume that the stars in both sequences follow an exponentially decreasing radial density profile given by

$$n(R) = k \exp\left(-\frac{R}{L}\right) \tag{8}$$

where R is the distance from the Galactic centre, L is the radial scale length, and k

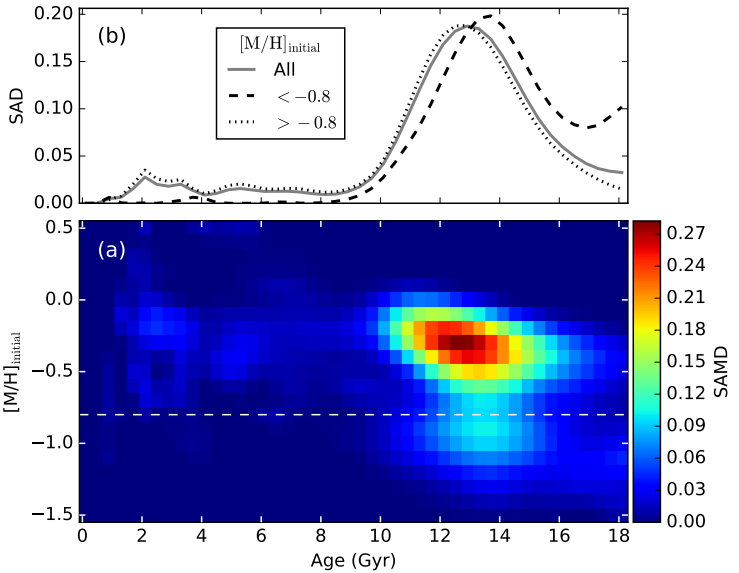

Figure 7: (a) SAMD and (b) SAD of 900 stars in GALAH DR3 with galactocentric azimuthal velocity below 120 km s^{-1}. The SAMD has a local minimum along the metallicity dimension at $[\mathrm{M/H}]_{\mathrm{initial}} = -0.8$ dex indicated by a dashed line. This minimum separates two peaks associated with accreted stars at low metallicities and kinematically hot disc stars, or *in situ* halo stars, at higher metallicities. The SAD is shown for the entire sample as well as for metallicities above and below the minimum at -0.8 dex. The accreted population is found to be slightly older on average than the *in situ* population for this particular sample selection. Adapted from Paper V.

is a normalization constant. This expression cannot be fitted directly to the observations due to the survey selection function dominating the spatial distribution of the sample. However, by assuming that stars in both the blue and red sequences are affected by the same selection function, the observed relative densities should correspond to the true values. By fitting the observed number densities to the expression $n_{\mathrm{red}}/n_{\mathrm{blue}}(R)$ with the scale lengths free to vary, we find a red sequence scale length of 2 to 3 kpc. The lower end of this range is comparable to the scale length of the Milky Way thick disc (Bland-Hawthorn & Gerhard, 2016). The scale length of the blue sequence, on the other hand, is in the range 30 to 60 kpc indicating an almost flat radial distribution within the observed volume. This is likely due to the highly radial orbits of these stars with apocenters at Galactocentric radii of up to 30 kpc (Deason et al., 2018).

In Paper V we investigated the SAMD of the turnoff stars in GALAH DR3

which includes a small number of halo stars. Belokurov et al. (2020) noted that the transition between what they define as the Splash and the thick disc is at an azimuthal velocity (in galactocentric cylindrical coordinates) $V_\phi \approx 100$ km s^{-1}. We increased this limit to 120 km s^{-1}, in order to get a significant sample size, and calculated the SAMD for all stars with an azimuthal velocity below this value. The resulting SAMD, shown in Figure 7, has two peaks at ages greater than 10 Gyr separated by a minimum in the metallicity distribution at $[\mathrm{M/H}]_{\mathrm{initial}} = -0.8$ dex. We interpret these peaks as corresponding to accreted stars at low metallicities and *in situ* stars from the kinematically hot tail of the disc at higher metallicities. The *in situ* population is found to be slightly younger than the accreted population; however, the difference is small and depends on the selection of the populations.

5.3 The modern zoo of halo substructures

So far we have discussed the existence of two main populations of halo stars: one accreted in the GSE merger and one formed *in situ* in the early Milky Way disc. These two populations, however, do not account for all stars on halo-like orbits. In addition to the halo substructures known prior to *Gaia*, like the Sagittarius stream, a large number of new structures have been identified in the past few years. One of the most prominent of these is a population of stars on highly retrograde orbits associated with the retrograde globular cluster FSR 1758. These stars are thought to originate in a dwarf galaxy named the Sequoia (Myeong et al., 2019) which is distinct from the GSE progenitor. In addition to being on different orbits, the Sequoia stars have a lower mean metallicity (-1.6 dex) than GSE stars. Koppelman et al. (2019) claim that Sequoia stars only occupy the high-energy retrograde orbits while the stars on retrograde orbits of lower energy belong to another distinct population they name Thamnos. Naidu et al. (2020) present four additional substructures, two of which further subdivides the retrograde halo population.

In Paper IV, we investigated the abundances and age distribution of Sequoia stars selected according to the definition of Myeong et al. (2019). The Sequoia stars do not appear to follow a single abundance sequence in the same way as the GSE stars (compare Figures 8a and 5). Instead, it looks like a mixture of populations with a significant fraction of the sample following what seems to be a low-metallicity extension of the thick disc. The SAD shown in Figure 8b has been derived in the same way as we did for the GSE (Figure 6), i.e. by applying the APOGEE metallicity distribution as a prior in the analysis of *Gaia* DR2 turnoff stars. The fact that the SAD has two old peaks is another indication that we are

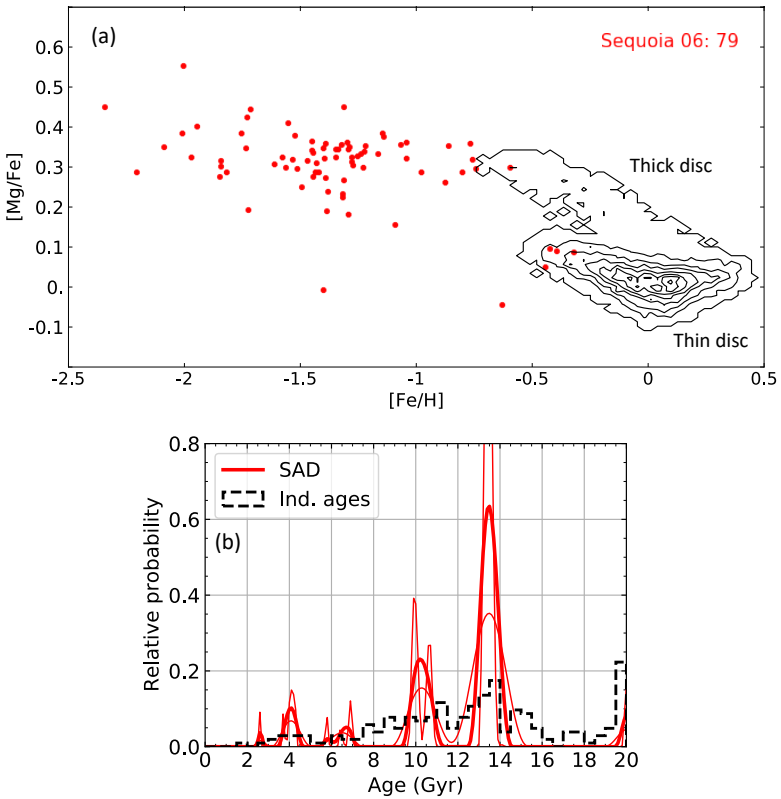

Figure 8: (a) Magnesium to iron abundance, $[\mathrm{Mg/Fe}]$, against metallicity, $[\mathrm{Fe/H}]$, for a selection of stars in APOGEE DR16. The red points show stars on highly retrograde orbits associated with the Sequoia population. The black contours indicate the distribution of Milky Way stars which can be divided into an alpha-rich and alpha-poor component (in this case magnesium is the alpha element), often associated with the thick and thin discs, respectively (see Section 6 for more details about the disc components). (b) Distribution of individual ages and SAD for Sequoia stars in *Gaia* DR2 selected kinematically like the APOGEE sample shown in panel a. The SAD is shown for three different values of the regularisation parameter: $\alpha = 0$, 2000 (thick line), 10^5. Regardless of the level of regularisation, the SAD shows two main peaks at ages greater than 9 Gyr which may indicate that Sequoia is a mixture of different stellar populations. Adapted from Paper IV.

seeing a mixed population.

Our results question the idea that Sequoia is a distinct population of stars accreted from a common progenitor; at least when defined simply as highly retrograde stars. Another recent study finds that the kinematics of the globular cluster FSR 1758 agree well with the definition of GSE (Romero-Colmenares et al., 2021). A possible alternative explanation for part of the Sequoia population is that it is made up of the low-metallicity GSE stars. One could imagine that the GSE dwarf galaxy had a negative radial metallicity gradient and that the outer low-metallicity stars were accreted onto retrograde orbits while the core collided head-on with the Milky Way (Helmi, 2020).

Whatever the origin of the retrograde stars, it is clear that there is still some uncertainty regarding the significance of the large number of recently identified halo substructures. This is only natural given the recent influx of data, and more work must be done in the future to robustly categorize stars beyond the two boxes labelled accreted and in-situ. To this end, age distributions can give some clues to the origin of substructures, as we have achieved for GSE and Sequoia. However, it is difficult to order these events chronologically with the current age precision and accuracy. Most Milky Way mergers are believed to have happened in the early universe ($\gtrsim$ 10 Gyr ago) (e.g. Ruchti et al., 2015) and at these ages most of our age distributions overlap heavily and possible systematic uncertainties can be significant relative to the differences we are attempting to quantify.

6 Formation of the stellar disc

The majority of stars in the Milky Way reside in the disc structure which can be divided geometrically into a thin and a thick component with scale heights of around 300 and 1000 pc, respectively (Gilmore & Reid, 1983; Bland-Hawthorn & Gerhard, 2016). The Sun is located close to the disc plane at a distance of about 8 kpc from the Galactic centre. Unlike halo stars which are almost exclusively old and metal-poor, stars in the disc cover a large range of parameters from ancient thick disc stars – some of which are on halo-like orbits as discussed in Section 5 – to the younger stars in the more metal-rich thin disc where star formation is still ongoing. The terms thin and thick disc are not only used in the geometrical sense, they are also used when referring to two populations with different elemental abundances and kinematics. For example, disc stars separate into two sequences in the [α/Fe] against [Fe/H] plane as shown in Figure 5. These sequences were first identified in the Solar neighbourhood and the high-alpha stars are found to be older and have larger vertical velocities (perpendicular to the disc plane) than the low-alpha stars (Fuhrmann, 1998; Bensby et al., 2003). Later studies of giant stars across the disc have found that the high-alpha sequence shows similar metallicities at all positions in the disc and that it is centrally concentrated, disappearing beyond 10 kpc from the Galactic centre (Nidever et al., 2014; Hayden et al., 2015). Low-alpha stars, on the other hand, are found across the disc with outwardly decreasing metallicities.

The low- and high-alpha stars are often referred to as chemically defined thin and thick disc stars. However, there is not a direct correlation between the chemically and geometrically defined disc components which can make the thin and thick disc terminology confusing (Hayden et al., 2017). Regardless of the definition of thin and thick disc components, any model of Galactic disc formation must be able to reproduce the trends found in elemental abundances and their correlation with stellar age. This section gives a short summary of a selection of disc formation models as well as the main results of Paper V in which we studied the relationship between age and metallicity of disc stars.

6.1 Disc formation models

One of the early attempts at reproducing the dual elemental abundance sequences of the Milky Way was made using a two-infall model (Chiappini et al., 1997). As the name suggests, this model considers two episodes of gas infall building up the stellar disc. The first infall results in a burst of star formation in which type II

supernovae dominate the chemical enrichment creating the high-alpha sequence on a timescale of about 1 Gyr. After a short pause in star formation, and the onset of type Ia supernovae, the second infall brings new low-metallicity gas which builds up the low-alpha sequence on a time scale of 8 Gyr. In a recent update of the model, the second infall is delayed by 4 Gyr to allow the metallicity to reach Solar values before the dilution by the second infall (Spitoni et al., 2019).

The two-infall model describes a scenario in which the thick (high-alpha) and thin (low-alpha) discs are distinct components that formed in a sequential manner. In another chemical evolution model, by Schönrich & Binney (2009), the two elemental abundance sequences arise without any dip in the star formation rate and without distinct gas infall episodes. Instead, it is a consequence of radial migration of stars bringing together stellar populations from different regions of the Galaxy where the chemical enrichment has proceeded at different rates. This leads to a Solar neighborhood population made up of high- and low-alpha stars primarily from the inner and outer disc, respectively.

In recent years the analytical models of chemical evolution have been supplemented by cosmological simulations of galaxy formation. Such simulations follow galaxy evolution all the way from the cosmologically informed initial conditions of the universe until the present day (see e.g., Naab & Ostriker, 2017). State of the art simulations are now able to produce Milky Way-like disc galaxies that show two sequences in $[\alpha/\mathrm{Fe}]$ against $[\mathrm{Fe/H}]$ similar to the observed ones (e.g., Grand et al., 2018; Buck, 2020; Agertz et al., 2021). In general, these simulations show chemical enrichment histories which are qualitatively similar to the two-infall model. That is, an initial central starburst forms the high-alpha sequence on a short time scale. Later on, a more extended disc forms out of a mixture of gas enriched by the initial starburst and metal-poor gas accreted from the surrounding medium. The source of the metal-poor gas, and the formation of the low-alpha sequence, differs between the simulations. Examples include a gas-rich merger diluting the gas left over from the initial starburst (Buck, 2020) and the formation of a distinct outer disc fed by metal-poor gas inflow (Agertz et al., 2021). Radial migration does redistribute stars in these simulations, but it is not the dominant mechanism behind the bimodal distribution of $[\alpha/\mathrm{Fe}]$.

6.2 The age-metallicity relation

In addition to the two $[\alpha/\mathrm{Fe}]$ sequences, the relationship between age and metallicity of disc stars is an important constraint on disc formation models. Studies of the age-metallicity relation in the Solar neighbourhood have shown that there

is no clear relation for stars younger than about 8 Gyr (Edvardsson et al., 1993; Casagrande et al., 2011). Instead, there is a large scatter in metallicity at all ages. This is consistent with a superposition of stars originating in different regions of the disc where the chemical enrichment has proceeded to different levels of metallicity at a given time. For the oldest stars, however, an age-metallicity relation has been found for stars selected kinematically to belong to the thick disc (Bensby et al., 2004) or selected to have high $[\alpha/\mathrm{Fe}]$ (Haywood et al., 2013). This is in line with the models discussed above since the initial starburst happens in a well-mixed medium giving a single chemical evolution sequence.

In Paper V we present the SAMD of almost 200 000 dwarf and subgiant stars in GALAH DR3. This is the first large-scale application of the method aimed at providing a more precise view of the age-metallicity distribution of Milky Way disc stars. With such a large sample we have also divided it kinematically into four subsamples. The four subsamples, Populations A to D, are divided according to the Galactocentric azimuthal velocity component, V_T,[4] as shown in Figure 9a. They correspond roughly to the kinematically defined halo (Population D), thick disc (Population C), and thin disc (Populations A and B). The SAMD of Population D was discussed in Section 5.2 and shows two peaks corresponding to the metal-poor accreted stars and the more metal-rich, kinematically hot disc stars.

The main result of this work is the identification of clear features and local minima in the SAMD which are not usually seen in age-metallicity scatter plots. One of these features is the clear age-metallicity relation seen in Population C which connects smoothly at the old end with the kinematically hot disc stars of Population D. The stars in Population C all belong to the inner disc, with mean Galactocentric radii $R_{\mathrm{mean}} \lesssim 7$ kpc.[5] This is consistent with the idea of an initial starburst in a well-mixed medium in the inner disc leading to a single well-defined chemical evolution sequence. Interestingly, there is a local minimum in the age distribution at 10 Gyr as seen in the SAD in Figure 9c. This minimum roughly separates the Population C stars with high and low $[\alpha/\mathrm{Fe}]$ (see Figure 9b) and also marks a transition from high to low vertical velocity dispersion. Only after this transition in Population C (the inner disc) does significant star formation begin in Population A which contains the outer disc stars with $R_{\mathrm{mean}} \gtrsim 9$ kpc. Thus, the outer disc started forming while the metallicity was still increasing in the inner

[4]Here we use V_T to denote the azimuthal velocity component because this is the notation used in the GALAH catalogue. It is, however, the same velocity component referred to as V_ϕ in Section 5.2.

[5]In this case the terms inner and outer are used in relation to the location of the Sun which in the GALAH catalogue is assumed to be at a Galactocentric radius of $R = 8.21$ kpc.

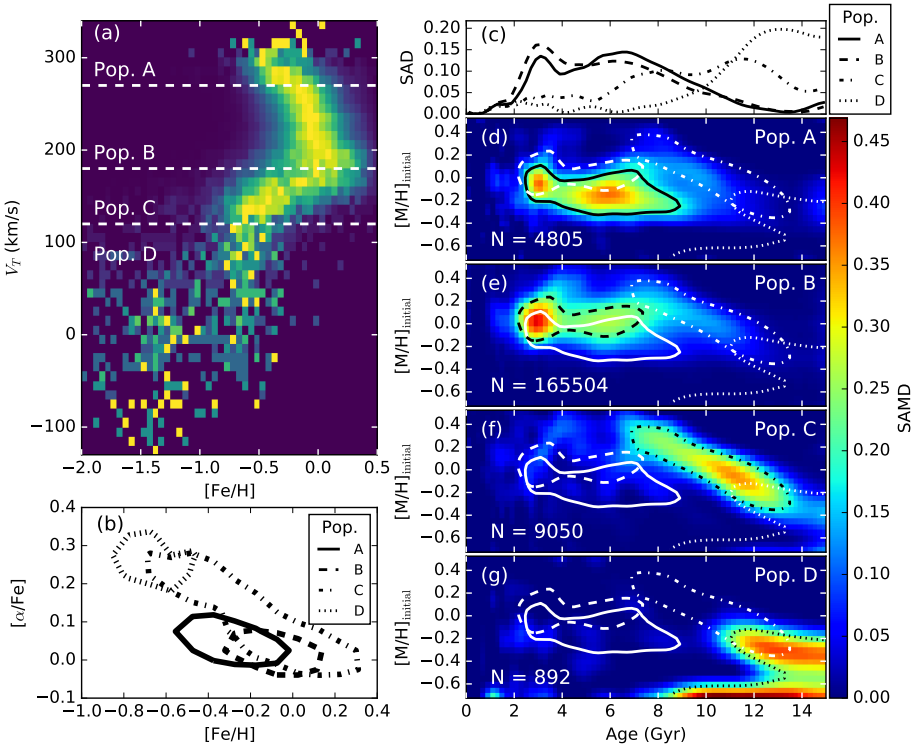

Figure 9: The SAMD and SAD of the GALAH sample in four different bins of Galactocentric azimuthal velocity, V_T. (a) V_T against [Fe/H] as a row-normalised 2D histogram. The dashed lines indicate the division between the four populations, A to D, at $V_T = 120$, 180, and 270 km s^{-1}. (b) Distribution of alpha abundance against metallicity for each population in the form of a half-of-maximum contour line. (c) SAD of the four populations. (d)-(g) SAMD of the four populations. In each panel the half-of-maximum contour line of the SAMD is shown in black and the contour lines from the other SAMDs are shown in white. Part of the SAMD of population D falls outside of the age-metallicity grid used in this figure, but it is shown in full in Figure 7. Adapted from Paper V.

disc. Populations A, C, and D can all be considered tails of the overall distribution of the sample. The vast majority of the sample is contained in Population B at V_T around the Solar value defined to be 248 km s^{-1} in the GALAH data. Stars in this population are found mainly at metallicities intermediate between the inner and outer populations.

Looking at the more recent history, there is a local minimum in the SAMD of Populations A and B at ages between 4 and 6 Gyr. The young peak between

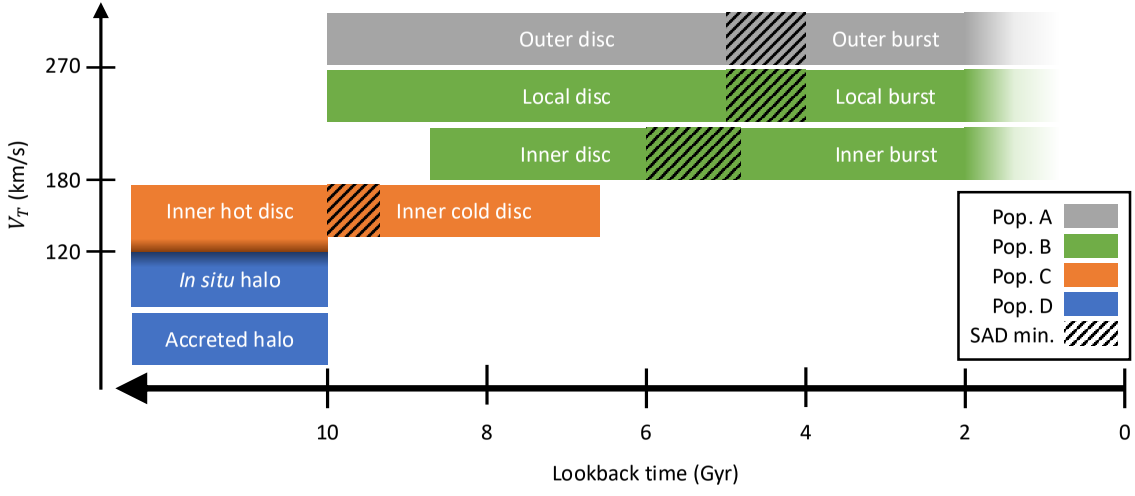

Figure 10: Schematic timeline giving an overview of the age distributions of the four kinematically selected subsamples shown in Figure 9. Populations C and D are connected at the old end to indicate that one transitions smoothly into the other in the inner disc. The hatched regions mark the approximate ages at which minima are found in the SAD. These minima, found at ages of about 5 and 10 Gyr divide the formation of the Milky Way disc into three main phases. Adapted from Paper V.

ages of 2 to 4 Gyr is consistent with studies using different tracers, such as white dwarfs, suggesting a recent burst of star formation in the disc (Mor et al., 2019; Isern, 2019). Peaks in the recent star formation history were also found by (Ruiz-Lara et al., 2020) based on CMD fitting of *Gaia* DR2 stars. They suggest that these periods of enhanced star formation were induced by pericentre passages of the Sagittarius dwarf galaxy. The greatest enhancement they find is at ages of 5.7 Gyr which is significantly older than the young peak in the SAMD, also when allowing for systematic age uncertainties on the level of 1 Gyr. Perhaps future studies comparing the results of the SAMD and CMD fitting can shed light on these differences.

The main results of Paper V can be summarised in terms of the schematic timeline shown in Figure 10. The timeline is divided into three main formation phases separated by the two local minima in the age distribution. In the first two phases, stars are formed with distinct kinematics and elemental abundances and separated by a local minimum in the age distribution at 10 Gyr. The last phase, a recent burst of star formation, is not clearly distinct in terms of stellar parameters but is marked by a local minimum in stellar age distribution.

This work comes in the wake of other observational studies arguing for distinct formation pathways of the inner and outer disc (Haywood et al., 2019; Ciucă et al., 2021). Together with this work, these studies indicate that the disc did form in at least two distinct phases resulting in the two alpha-abundance sequences. One of the challenges for the future is to work out the detailed circumstances surrounding the transition from an inner starburst to a more extended star formation. The halo formation scenario discussed in Section 5 could explain the transition as being the time of the GSE merger. Such a scenario is supported by at least one cosmological galaxy simulation in which a GSE-like merger heats the existing disc stars (creating the Splash population), brings in new metal-poor gas, and induces star formation in a thin component (Bignone et al., 2019). On the other hand, the transition could be caused by secular processes like the end of an early phase of high star formation rate in dense star forming clumps (Clarke et al., 2019; Amarante et al., 2020).

7 Outlook

The high level of activity currently seen in the field of Galactic Archaeology is likely to continue for many years to come. In some sense, the era of large surveys has only just begun, and a number of large-scale surveys of stars in the Milky Way will begin observing in the near future. On the side of spectroscopy, surveys like the WHT Enhanced Area Velocity Explorer (WEAVE) and the 4-metre Multi-Object Spectroscopic Telescope (4MOST; de Jong et al., 2016) are set to provide elemental abundance data for a combined 20 million stars across the northern (WEAVE) and southern (4MOST) hemisphere.

Of particular interest for age estimation is the coming seismic data from the Transiting Exoplanet Survey Satellite (TESS; Ricker et al., 2015) and the Planetary Transits and Oscillations of Stars mission (PLATO; Rauer et al., 2016). These missions are primarily focused on exoplanetary science, but the long and precise time series photometry necessary for characterizing exoplanet transits are also well suited for studying stellar oscillations. The first seismic analysis of TESS data has shown that relative age precisions of 20 per cent are achievable for oscillating giant stars (Silva Aguirre et al., 2020). In total these missions are expected to increase the number of stars with detected oscillations by at least a factor of ten (Hon et al., 2021). This seismic data is useful for age estimation of the oscillating stars themselves, but also as an expansion of the training samples used in machine learning methods for age determination of giant stars.

In light of this upcoming data it would be interesting to apply the SAMD-method presented in this work to a sample of giants with seismic age estimates. In Paper III we carried out a single test applying the method to synthetic data including seismic parameters. This test showed that it can recover the age distribution of seismic giants more precisely than the distribution of individual seismic ages, especially for the oldest stars. If this carries over to samples of real stars, we could potentially obtain precise age distributions for stars in a wider volume of the Galaxy than we have been able to using GALAH dwarfs and subgiants.

The SAMD method could also be expanded to include other parameters. The most obvious extension would be to include the alpha-element abundance as a model parameter and study the age-alpha relation of different stellar populations. The method is also not restricted to age estimates from model fitting. In principle, the $\mathcal{G}$-function in Eq. (7) can be any age-metallicity (or just age) probability density function. An interesting prospect is to combine the method with age estimates from machine learning methods calibrated on seismic ages. Such age estimates are available for hundreds of thousands of stars based on their spectra, but only in

the form of point estimates. If we can find a way to express these estimates in the form of probability density functions it might be possible to get more precise age information out of this great source of data.

While the amount of data is increasing and data analysis methods are improving, galaxy models are also becoming more sophisticated. High-resolution cosmological simulations open up the possibility of detailed comparisons between models and observations. Such comparisons have been made in a qualitative sense in this work (mainly in Paper V), and in the future it would be interesting to make detailed quantitative comparisons, for example, between the age distributions of stars in different regions of the Galaxy. Of course, any given simulation is just one realisation of a model galaxy and is therefore not expected to match the observations perfectly. But perhaps future advances in computational power can provide us with large enough samples of high-resolution simulations that they can be compared with Milky Way observations in a statistical sense.

All things considered, it is easy to imagine that our understanding of the formation and evolution of the Milky Way will continue to improve rapidly in the coming decades.

References

Agertz, O., Renaud, F., Feltzing, S., et al. 2021, MNRAS, 503, 5826, doi: 10.1093/mnras/stab322

Ahumada, R., Prieto, C. A., Almeida, A., et al. 2020, ApJS, 249, 3, doi: 10.3847/1538-4365/ab929e

Amarante, J. A. S., Beraldo e Silva, L., Debattista, V. P., & Smith, M. C. 2020, ApJL, 891, L30, doi: 10.3847/2041-8213/ab78a4

Angus, R., Aigrain, S., Foreman-Mackey, D., & McQuillan, A. 2015, MNRAS, 450, 1787, doi: 10.1093/mnras/stv423

Astraatmadja, T. L., & Bailer-Jones, C. A. L. 2016, ApJ, 832, 137, doi: 10.3847/0004-637X/832/2/137

Bailer-Jones, C. A. L., Rybizki, J., Fouesneau, M., Mantelet, G., & Andrae, R. 2018, AJ, 156, 58, doi: 10.3847/1538-3881/aacb21

Barnes, S. A. 2003, ApJ, 586, 464, doi: 10.1086/367639

—. 2007, ApJ, 669, 1167, doi: 10.1086/519295

Barnes, S. A., Weingrill, J., Fritzewski, D., Strassmeier, K. G., & Platais, I. 2016, ApJ, 823, 16, doi: 10.3847/0004-637X/823/1/16

Belokurov, V., Erkal, D., Evans, N. W., Koposov, S. E., & Deason, A. J. 2018, MNRAS, 478, 611, doi: 10.1093/mnras/sty982

Belokurov, V., Sanders, J. L., Fattahi, A., et al. 2020, MNRAS, 494, 3880, doi: 10.1093/mnras/staa876

Bennett, C. L., Larson, D., Weiland, J. L., et al. 2013, ApJS, 208, 20, doi: 10.1088/0067-0049/208/2/20

Bensby, T., Feltzing, S., & Lundström, I. 2003, A&A, 410, 527, doi: 10.1051/0004-6361:20031213

—. 2004, A&A, 421, 969, doi: 10.1051/0004-6361:20035957

Bignone, L. A., Helmi, A., & Tissera, P. B. 2019, ApJL, 883, L5, doi: 10.3847/2041-8213/ab3e0e

Bland-Hawthorn, J., & Gerhard, O. 2016, ARA&A, 54, 529, doi: 10.1146/annurev-astro-081915-023441

Bonaca, A., Conroy, C., Wetzel, A., Hopkins, P. F., & Kereš, D. 2017, ApJ, 845, 101, doi: 10.3847/1538-4357/aa7d0c

Bovy, J. 2015, ApJS, 216, 29, doi: 10.1088/0067-0049/216/2/29

Bressan, A., Marigo, P., Girardi, L., et al. 2012, MNRAS, 427, 127, doi: 10.1111/j.1365-2966.2012.21948.x

Buck, T. 2020, MNRAS, 491, 5435, doi: 10.1093/mnras/stz3289

Buder, S., Sharma, S., Kos, J., et al. 2021, MNRAS, 506, 150, doi: 10.1093/mnras/stab1242

Casagrande, L., Schönrich, R., Asplund, M., et al. 2011, A&A, 530, A138, doi: 10.1051/0004-6361/201016276

Casagrande, L., Wolf, C., Mackey, A. D., et al. 2019, MNRAS, 482, 2770, doi: 10.1093/mnras/sty2878

Chaplin, W. J., & Miglio, A. 2013, ARA&A, 51, 353, doi: 10.1146/annurev-astro-082812-140938

Chiappini, C., Matteucci, F., & Gratton, R. 1997, ApJ, 477, 765, doi: 10.1086/303726

Choi, J., Dotter, A., Conroy, C., et al. 2016, ApJ, 823, 102, doi: 10.3847/0004-637X/823/2/102

Ciucă, I., Kawata, D., Miglio, A., Davies, G. R., & Grand, R. J. J. 2021, MNRAS, 503, 2814, doi: 10.1093/mnras/stab639

Clarke, A. J., Debattista, V. P., Nidever, D. L., et al. 2019, MNRAS, 484, 3476, doi: 10.1093/mnras/stz104

de Jong, R. S., Barden, S. C., Bellido-Tirado, O., et al. 2016, in Society of Photo-Optical Instrumentation Engineers (SPIE) Conference Series, Vol. 9908, Ground-based and Airborne Instrumentation for Astronomy VI, ed. C. J. Evans, L. Simard, & H. Takami, 99081O, doi: 10.1117/12.2232832

De Silva, G. M., Freeman, K. C., Bland-Hawthorn, J., et al. 2015, MNRAS, 449, 2604, doi: 10.1093/mnras/stv327

Deason, A. J., Belokurov, V., Koposov, S. E., & Lancaster, L. 2018, ApJL, 862, L1, doi: 10.3847/2041-8213/aad0ee

Demarque, P., Woo, J.-H., Kim, Y.-C., & Yi, S. K. 2004, ApJS, 155, 667, doi: 10.1086/424966

Di Matteo, P., Haywood, M., Lehnert, M. D., et al. 2019, A&A, 632, A4, doi: 10.1051/0004-6361/201834929

Dolphin, A. E. 2002, MNRAS, 332, 91, doi: 10.1046/j.1365-8711.2002.05271.x

Dotter, A. 2016, ApJS, 222, 8, doi: 10.3847/0067-0049/222/1/8

Dotter, A., Conroy, C., Cargile, P., & Asplund, M. 2017, ApJ, 840, 99, doi: 10.3847/1538-4357/aa6d10

Edvardsson, B., Andersen, J., Gustafsson, B., et al. 1993, A&A, 500, 391

Eggen, O. J., Lynden-Bell, D., & Sandage, A. R. 1962, ApJ, 136, 748, doi: 10.1086/147433

Feuillet, D. K., Feltzing, S., Sahlholdt, C. L., & Casagrande, L. 2020, MNRAS, 497, 109, doi: 10.1093/mnras/staa1888

Freeman, K., & Bland-Hawthorn, J. 2002, ARA&A, 40, 487, doi: 10.1146/annurev.astro.40.060401.093840

Fuhrmann, K. 1998, A&A, 338, 161

Gaia Collaboration, Prusti, T., de Bruijne, J. H. J., et al. 2016, A&A, 595, A1, doi: 10.1051/0004-6361/201629272

Gaia Collaboration, Brown, A. G. A., Vallenari, A., et al. 2018a, A&A, 616, A1, doi: 10.1051/0004-6361/201833051

Gaia Collaboration, Babusiaux, C., van Leeuwen, F., et al. 2018b, A&A, 616, A10, doi: 10.1051/0004-6361/201832843

Gaia Collaboration, Brown, A. G. A., Vallenari, A., et al. 2021, A&A, 649, A1, doi: 10.1051/0004-6361/202039657

Gallart, C., Bernard, E. J., Brook, C. B., et al. 2019, Nature Astronomy, 3, 932, doi: 10.1038/s41550-019-0829-5

Gallart, C., Zoccali, M., & Aparicio, A. 2005, ARA&A, 43, 387, doi: 10.1146/annurev.astro.43.072103.150608

Gilmore, G., & Reid, N. 1983, MNRAS, 202, 1025, doi: 10.1093/mnras/202.4.1025

Grand, R. J. J., Bustamante, S., Gómez, F. A., et al. 2018, MNRAS, 474, 3629, doi: 10.1093/mnras/stx3025

Hayden, M. R., Recio-Blanco, A., de Laverny, P., Mikolaitis, S., & Worley, C. C. 2017, A&A, 608, L1, doi: 10.1051/0004-6361/201731494

Hayden, M. R., Bovy, J., Holtzman, J. A., et al. 2015, ApJ, 808, 132, doi: 10.1088/0004-637X/808/2/132

Haywood, M., Di Matteo, P., Lehnert, M. D., Katz, D., & Gómez, A. 2013, A&A, 560, A109, doi: 10.1051/0004-6361/201321397

Haywood, M., Di Matteo, P., Lehnert, M. D., et al. 2018, ApJ, 863, 113, doi: 10.3847/1538-4357/aad235

Haywood, M., Snaith, O., Lehnert, M. D., Di Matteo, P., & Khoperskov, S. 2019, A&A, 625, A105, doi: 10.1051/0004-6361/201834155

Heiter, U., Jofré, P., Gustafsson, B., et al. 2015, A&A, 582, A49, doi: 10.1051/0004-6361/201526319

Helmi, A. 2008, A&A Rv, 15, 145, doi: 10.1007/s00159-008-0009-6

—. 2020, ARA&A, 58, 205, doi: 10.1146/annurev-astro-032620-021917

Helmi, A., Babusiaux, C., Koppelman, H. H., et al. 2018, Nature, 563, 85, doi: 10.1038/s41586-018-0625-x

Hernandez, X., Valls-Gabaud, D., & Gilmore, G. 1999, MNRAS, 304, 705, doi: 10.1046/j.1365-8711.1999.02102.x

—. 2000, MNRAS, 316, 605, doi: 10.1046/j.1365-8711.2000.03537.x

Ho, A. Y. Q., Rix, H.-W., Ness, M. K., et al. 2017, ApJ, 841, 40, doi: 10.3847/1538-4357/aa6db3

Hon, M., Huber, D., Kuszlewicz, J. S., et al. 2021, arXiv e-prints, arXiv:2108.01241. https://arxiv.org/abs/2108.01241

Howes, L. M., Lindegren, L., Feltzing, S., Church, R. P., & Bensby, T. 2019, A&A, 622, A27, doi: 10.1051/0004-6361/201833280

Ibata, R. A., Gilmore, G., & Irwin, M. J. 1994, Nature, 370, 194, doi: 10.1038/370194a0

Ibukiyama, A., & Arimoto, N. 2002, A&A, 394, 927, doi: 10.1051/0004-6361:20021157

Isern, J. 2019, ApJL, 878, L11, doi: 10.3847/2041-8213/ab238e

Jofré, P., Heiter, U., Soubiran, C., et al. 2014, A&A, 564, A133, doi: 10.1051/0004-6361/201322440

Jönsson, H., Holtzman, J. A., Allende Prieto, C., et al. 2020, AJ, 160, 120, doi: 10.3847/1538-3881/aba592

Jørgensen, B. R., & Lindegren, L. 2005a, A&A, 436, 127, doi: 10.1051/0004-6361:20042185

Jørgensen, B. R., & Lindegren, L. 2005b, in ESA Special Publication, Vol. 576, The Three-Dimensional Universe with Gaia, ed. C. Turon, K. S. O'Flaherty, & M. A. C. Perryman, 171

Jørgensen, B. R. 2005, PhD thesis, Lund University

Koppelman, H., Helmi, A., & Veljanoski, J. 2018, ApJL, 860, L11, doi: 10.3847/2041-8213/aac882

Koppelman, H. H., Helmi, A., Massari, D., Price-Whelan, A. M., & Starkenburg, T. K. 2019, A&A, 631, L9, doi: 10.1051/0004-6361/201936738

Mackereth, J. T., Schiavon, R. P., Pfeffer, J., et al. 2019, MNRAS, 482, 3426, doi: 10.1093/mnras/sty2955

Majewski, S. R., Skrutskie, M. F., Weinberg, M. D., & Ostheimer, J. C. 2003, ApJ, 599, 1082, doi: 10.1086/379504

Majewski, S. R., Schiavon, R. P., Frinchaboy, P. M., et al. 2017, AJ, 154, 94, doi: 10.3847/1538-3881/aa784d

Mamajek, E. E., & Hillenbrand, L. A. 2008, ApJ, 687, 1264, doi: 10.1086/591785

Meibom, S., Barnes, S. A., Platais, I., et al. 2015, Nature, 517, 589, doi: 10.1038/nature14118

Mints, A., Hekker, S., & Minchev, I. 2019, A&A, 629, A127, doi: 10.1051/0004-6361/201935864

Mor, R., Robin, A. C., Figueras, F., Roca-Fàbrega, S., & Luri, X. 2019, A&A, 624, L1, doi: 10.1051/0004-6361/201935105

Myeong, G. C., Vasiliev, E., Iorio, G., Evans, N. W., & Belokurov, V. 2019, MNRAS, 488, 1235, doi: 10.1093/mnras/stz1770

Naab, T., & Ostriker, J. P. 2017, ARA&A, 55, 59, doi: 10.1146/annurev-astro-081913-040019

Naidu, R. P., Conroy, C., Bonaca, A., et al. 2020, ApJ, 901, 48, doi: 10.3847/1538-4357/abaef4

Ness, M., Hogg, D. W., Rix, H. W., et al. 2016, ApJ, 823, 114, doi: 10.3847/0004-637X/823/2/114

Ng, Y. K., & Bertelli, G. 1998, A&A, 329, 943. https://arxiv.org/abs/astro-ph/9707043

Nidever, D. L., Bovy, J., Bird, J. C., et al. 2014, ApJ, 796, 38, doi: 10.1088/0004-637X/796/1/38

Nissen, P. E. 2015, A&A, 579, A52, doi: 10.1051/0004-6361/201526269

—. 2016, A&A, 593, A65, doi: 10.1051/0004-6361/201628888

Nissen, P. E., & Schuster, W. J. 2010, A&A, 511, L10, doi: 10.1051/0004-6361/200913877

Pinsonneault, M. H., Elsworth, Y., Epstein, C., et al. 2014, ApJS, 215, 19, doi: 10.1088/0067-0049/215/2/19

Pont, F., & Eyer, L. 2004, MNRAS, 351, 487, doi: 10.1111/j.1365-2966.2004.07780.x

Porto de Mello, G. F., da Silva, R., da Silva, L., & de Nader, R. V. 2014, A&A, 563, A52, doi: 10.1051/0004-6361/201322277

Rauer, H., Aerts, C., Cabrera, J., & PLATO Team. 2016, Astronomische Nachrichten, 337, 961, doi: 10.1002/asna.201612408

Ricker, G. R., Winn, J. N., Vanderspek, R., et al. 2015, Journal of Astronomical Telescopes, Instruments, and Systems, 1, 014003, doi: 10.1117/1.JATIS.1.1.014003

Robin, A. C., Reylé, C., Derrière, S., & Picaud, S. 2003, A&A, 409, 523, doi: 10.1051/0004-6361:20031117

Romero-Colmenares, M., Fernández-Trincado, J. G., Geisler, D., et al. 2021, arXiv e-prints, arXiv:2106.00027. https://arxiv.org/abs/2106.00027

Ruchti, G. R., Read, J. I., Feltzing, S., et al. 2015, MNRAS, 450, 2874, doi: 10.1093/mnras/stv807

Ruiz-Lara, T., Gallart, C., Bernard, E. J., & Cassisi, S. 2020, Nature Astronomy, 4, 965, doi: 10.1038/s41550-020-1097-0

Salaris, M., Chieffi, A., & Straniero, O. 1993, ApJ, 414, 580, doi: 10.1086/173105

Salpeter, E. E. 1955, ApJ, 121, 161, doi: 10.1086/145971

Sanders, J. L., & Das, P. 2018, MNRAS, 481, 4093, doi: 10.1093/mnras/sty2490

Schönrich, R., & Bergemann, M. 2014, MNRAS, 443, 698, doi: 10.1093/mnras/stu1072

Schönrich, R., & Binney, J. 2009, MNRAS, 396, 203, doi: 10.1111/j.1365-2966.2009.14750.x

Schönrich, R., McMillan, P., & Eyer, L. 2019, MNRAS, 487, 3568, doi: 10.1093/mnras/stz1451

Searle, L., & Zinn, R. 1978, ApJ, 225, 357, doi: 10.1086/156499

Silva Aguirre, V., Lund, M. N., Antia, H. M., et al. 2017, ApJ, 835, 173, doi: 10.3847/1538-4357/835/2/173

Silva Aguirre, V., Bojsen-Hansen, M., Slumstrup, D., et al. 2018, MNRAS, 475, 5487, doi: 10.1093/mnras/sty150

Silva Aguirre, V., Stello, D., Stokholm, A., et al. 2020, ApJL, 889, L34, doi: 10.3847/2041-8213/ab6443

Skrutskie, M. F., Cutri, R. M., Stiening, R., et al. 2006, AJ, 131, 1163, doi: 10.1086/498708

Small, E. E., Bersier, D., & Salaris, M. 2013, MNRAS, 428, 763, doi: 10.1093/mnras/sts077

Soderblom, D. R. 2010, ARA&A, 48, 581, doi: 10.1146/annurev-astro-081309-130806

Spina, L., Meléndez, J., Karakas, A. I., et al. 2016, A&A, 593, A125, doi: 10.1051/0004-6361/201628557

Spitoni, E., Silva Aguirre, V., Matteucci, F., Calura, F., & Grisoni, V. 2019, A&A, 623, A60, doi: 10.1051/0004-6361/201834188

Strömgren, B. 1966, ARA&A, 4, 433, doi: 10.1146/annurev.aa.04.090166.002245

Tinsley, B. M. 1979, ApJ, 229, 1046, doi: 10.1086/157039

Tolstoy, E., & Saha, A. 1996, ApJ, 462, 672, doi: 10.1086/177181

Tosi, M., Greggio, L., Marconi, G., & Focardi, P. 1991, AJ, 102, 951, doi: 10.1086/115925

Tucci Maia, M., Ramírez, I., Meléndez, J., et al. 2016, A&A, 590, A32, doi: 10.1051/0004-6361/201527848

Valenti, J. A., & Fischer, D. A. 2005, ApJS, 159, 141, doi: 10.1086/430500

van Saders, J. L., Ceillier, T., Metcalfe, T. S., et al. 2016, Nature, 529, 181, doi: 10.1038/nature16168

Wright, J. T., Marcy, G. W., Butler, R. P., & Vogt, S. S. 2004, ApJS, 152, 261, doi: 10.1086/386283

Scientific publications

Author contributions

Co-authors are abbreviated as follows:
Luca Casagrande (LC), Ross P. Church (RPC), Sofia Feltzing (SF), Diane Feuillet (DF), Lennart Lindegren (LL).

Paper I

SF provided the original idea for the project and SF and **CLS** decided on its direction. **CLS** performed the collection of literature data with help from SF to sort through the sources. LL provided the first version of the code for age estimation which **CLS** adapted to Python. **CLS** performed the analysis and the results were interpreted together with SF, LL, and RPC. The manuscript was written mainly by **CLS** with a paragraph by LL in section 3.1. SF, LL, and RPC provided comments and corrections for the final manuscript.

Paper II

SF provided the original idea for the project and LC provided the SkyMapper data. Most of the analysis was carried out by **CLS** with frequent input from SF and LC. **CLS** wrote the manuscript with SF providing a paragraph in section 2.1 and writing the discussion in section 3.5. SF and LC provided comments and corrections for the final manuscript.

Paper III

The idea to carry out this project developed between **CLS** and LL based on previous work by LL. LL came up with the method and **CLS** developed the Python implementation with some adaptions to the original method along the way. **CLS**

created the synthetic data and, together with LL, defined the tests to carry out. The analysis was carried out by **CLS**. **CLS** wrote the manuscript with LL providing comments and corrections on the final version.

Paper IV

DF proposed the project as a continuation of previous work on halo populations. The direction of the project mainly developed during meetings between DF, **CLS**, and SF. DF carried out the analysis and wrote the majority of the manuscript. **CLS** wrote section 4.3.2 on age estimation, with input from DF, and created Figures 7 and 8. **CLS**, SF, and LC provided comments on the final manuscript.

Paper V

CLS proposed the project as an application of the method developed in paper III. The direction of the project was set during regular meetings with SF and DF who provided suggestions for the analysis. **CLS** collected the data and carried out the analysis. The manuscript was written by **CLS** with frequent input from SF and DF.